Review

Integrated photo-rechargeable energy storage system: next-generation power source driving the future

Qiang Zeng, Yanqing Lai, Liangxing Jiang, Fangyang Liu, Xiaojing Hao,* Lianzhou Wang,* Martin A. Green*

Dr. Qiang Zeng, Dr. Yanqing Lai, Prof. Fangyang Liu

School of Metallurgy and Environment, Central South University, Changsha 410083, P. R. China.

E-mail: liufangyang@csu.edu.cn

Dr. Liangxing Jiang

Engineering Research Centre of Advanced Battery Materials, Ministry of Education, Changsha 410083, P. R. China.

Prof. Xiaojing Hao, Prof. Martin A. Green

Australian Centre for Advanced Photovoltaics, School of Photovoltaic and Renewable Energy Engineering, University of New South Wales, NSW 2052, Australia

E-mail: xj.hao@unsw.edu.au

Prof. Lianzhou Wang

Nanomaterials Centre, School of Chemical Engineering, The University of Queensland, QLD 4072, Australia

E-mail: l.wang@uq.edu.au

Key words: photo-rechargeable, supercapacitors, static batteries, flow batteries, solar cells, photoelectrodes

Abstract: Solar energy is one of the most abundant renewable energy sources. For efficient utilization of solar energy, photovoltaic technology is regarded as the most important source. However, due to the intermittent and unstable characteristics of solar radiation, photoelectric conversion (PC) devices fail to meet the requirement of continuous power output. With the development of rechargeable electric energy storage systems (ESSs) (e.g., supercapacitors and batteries), the integration of a PC device and a rechargeable ESS has become a promising approach to solving this problem. The so-called integrated photo-rechargeable ESSs which can directly store sunlight generated electricity in daylight and reversibly release it at night time has a huge potential for future applications. This review summarizes the development of several types of mainstream integrated photo-rechargeable ESSs and introduces different

working mechanisms for each photo-rechargeable ESS in detail. Several general perspectives on the challenges and future development are also provided.

1. Introduction

The global demand for energy is significantly increasing with the development of human society. The limited capacity and pollutant emission from traditional fossil fuel have become two major global problems. For long-term energy needs and environmentally sustainable development, renewable energies are the most promising solutions for addressing these concerns.[1] Among various energy resources, solar energy is virtually unlimited and regarded as the most crucial need for the future.[2] Photoelectric conversion (PC) technology achieving the direct conversion of solar energy to electricity has been recognized as one of the most effective and sustainable methods.[3, 4] PC devices such as solar cells with increasing efficiency and decreasing cost have been widely employed for electricity generation. However, the intermittence of solar energy makes it an unreliable source to fulfill the energy demand at all times.

The mitigation of such a challenge lies in the combination of PC devices with electric energy storage systems (ESSs).[5] Photo-rechargeable ESSs could convert solar energy to electric energy and reversibly store electric energy in the form of chemical energy. So far, the most common way of charging a rechargeable ESS device by a PC unit is via the direct wire connection of two individual devices.[6] Like typical commercial portable power sources incorporated with silicon solar cells to realize self-charging, they are essentially composed of

two independent devices and simply connected by a control circuit. Consequently they suffer from energy mismatch and low levels of integration requiring long-distance wiring and complicated circuitry, tending to be bulky, inflexible, and low efficiency.[7] The photo-rechargeable ESSs integrating PC units with rechargeable ESSs have therefore recently emerged as an attractive alternative solutions to realize energy conversion and storage in a single device.[8] These integrated photo-rechargeable ESSs have advantages of small volume, light-weight, flexibility, and high-security.[2, 5] The above-mentioned PC units can be classified into two categories: solar cells and photoelectrodes. In other words, under light illumination, the light-converted electric energy is directly stored in the ESSs through two integrated forms: i) integrating an individual solar cell with ESS,[9] in which a common electrode is usually used for energy conversion part and storage part, as depicted in **figure 1a**; ii) incorporating dual-functional photoelectrodes into an ESS,[10] in which the employed photoelectrodes not only convert light to electricity but also have an electric energy storage function, as depicted in **figure 1b**. To evaluate the performance of photo-rechargeable ESSs, the solar-to-output energy conversion and storage efficiency (overall efficiency or $\eta_{overall}$ for short) is widely used as the key parameter, which can be obtained from following formula:[11]

$$\eta_{overall} = \frac{E_{output}}{E_{light}} \times 100\% \quad (1)$$

where the E_{light} and E_{output} are input energy from light and output energy from rechargeable ESS, respectively.

There are three stages that determine the overall efficiency: solar to electric energy conversion, electric to chemical energy conversion (photo-charging process) and reversible chemical to electric energy conversion (discharge process). Among those, the efficiency of electric to chemical energy conversion is the most crucial factor for the whole device, which may limit the overall efficiency due to the incompatible current–voltage features between PC

units and ESSs.[12] Thereby, the matching of parameters like voltage, current, energy, power and lifetime is needed for reasonable operation. For solar cell based integrated devices, the power conversion efficiency (PCE) and maximum power point (MPP) under one sun illumination (AM 1.5, 100 mW cm^{-2}) of solar cells undoubtedly are significant factors for the overall performance of photo-rechargeable ESS devices.[4] Different from the wire-connected photo-rechargeable ESSs, in which a rectifier can be connected between solar cells and ESSs,[7] for the integrated photo-rechargeable ESSs, the output features of solar cells and charging parameters of ESSs require to be closely matched. For photoelectrode based photo-rechargeable ESSs, in addition to the above-mentioned parameters matching, the photoelectrochemical mechanisms between semiconductor photoelectrodes and electrolytes need to be considered.

Based on the different energy storage mechanisms and capacity, herein, the mainstream rechargeable ESSs are divided into supercapacitors with high charge/discharge rates and redox batteries with high energy density. Further, to subdivide the multitudinous batteries, rechargeable static batteries with at least one solid charge storage electrode and redox flow batteries with energy storage in the liquid electrolyte are distinguished. Considering the integrated photo-rechargeable ESSs based on these three types of rechargeable ESSs could have different photo-charging and energy-storage features. In this article, we provide an overview of photo-rechargeable ESSs from the aspect of different energy storage devices. For each photo-rechargeable ESS, the photo-charging process by solar cells or photoelectrodes is reviewed in-depth. The crucial challenge of parameters matching and the potential application field for each photo-rechargeable ESS are also discussed which is distinct from previous reviews. In the end, we propose a test standard for photo-rechargeable ESSs to evaluate the overall efficiency. Also several perspectives on the future development of photo-rechargeable ESSs are listed.

2. Photo-rechargeable supercapacitors

Supercapacitors (SCs), also known as electrochemical capacitors, have been often used to store electrical energy in recent years. Based on the charge storage mechanism, SCs are classified into two types: electric double-layer (EDL) capacitors and pseudocapacitors.[13] The EDL capacitors store charges on active materials with high specific surface area through electrostatic force, while the pseudocapacitors store charges by means of a fast and reversible redox reaction at the electrode surfaces. Owing to these two storage mechanisms, SCs have outstanding properties such as high charge/discharge rates and long cycle life. Consequently, photo-rechargeable SCs (photocapacitors), in which the SCs are integrated with PC units, have provided a promising strategy to realize fast energy conversion and storage in a single device.[14] The concept of photocapacitors can be dated back to 2004[15] and has witnessed a rapid development in recent years. Reviewing the progress of photocapacitors, we can categorize all photocapacitors into two groups according to the types of PC units. The first group is integration of SCs and individual solar cells (such as dye-sensitized solar cells (DSSCs), perovskite solar cells (PSCs) and organic solar cells (OSCs)). The second group is incorporating a photoelectrode with a dual-function of photoelectric conversion and charge storage in SCs. For example, some pseudocapacitive semiconductor materials could be selected for this dual-functional photoelectrode.

2.1 Integration of SCs and solar cells

2.1.1 Dye-sensitized solar cells

Dye-sensitized solar cells (DSSCs) with many features like simple device configuration, facile manufacturing processes, and relative fast photoinduced redox reaction are suitable for

photo-charging SCs.[16, 17] Dye-sensitized photocapacitors (DS-photocapacitors) have attracted many investigations over the past decade. In 2004, Miyasaka et al. reported the first prototype of DS-photocapacitor in which a dye-coated TiO_2 layer was directly attached on an active carbon layer as shown in **figure 2a**.[15] In this two-electrode photocapacitor, the electrons and holes were generated from the dye molecules under light irradiation. The electrons were then collected by TiO_2 and transported to the counter electrode through an external circuit, and the holes flowed to active carbon through a chemical reaction with LiI: Dye (hole$^+$) + LiI → Dye + Li^++ 1/2I_2. These photo-generated carriers induced charge accumulation on the microporous surface of activated carbon, reaching a charging voltage of 0.45V and a specific areal capacitance of 0.69 F cm^{-2}. This work demonstrated the feasibility of photo-charging a supercapacitor and aroused significant interests in the investigation of photocapacitors. One year later, the above team developed a three-electrode photocapacitor to decrease the internal resistance which retarded the discharge process in a two-electrode photocapacitor.[18] The three-electrode photocapacitor integrated a dye-sensitized solar cell and an activated carbon supercapacitor through a common electrode. Herein, the common electrode is composed of a Pt electrode and a carbon electrode, as shown in **figure 2b**. During the photo-charging progress, photo-generated electrons and holes from the dye-coated photoelectrode transported to the counter electrode through external circuit and to the common electrode through electrolytes, respectively. Discharge of the photocapacitor was carried out through the external circuit combining the common electrode and counter electrode, which acted as positively and negatively charged electrodes, respectively. This three-electrode photocapacitor attained a charge-state voltage of 0.8 V and high energy density of 47 μW h cm^{-2} during the first cycle, which was higher than that attained in the previous two-electrode photocapacitor, indicating that the three-electrode configuration with a common electrode facilitated electron and hole transfer in the charge–discharge processes.

Therefore, for DS-photocapacitors, an outstanding common electrode play a critical role in for connection of DSSC and SCs, such as decreasing internal resistance. In addition, some materials used as a common electrode in three-electrode configuration can possess the dual-function of catalysis for DSSCs (similar to Pt electrode) and charge storage for SCs. Carbon materials have been widely used as electrodes in SCs owing to high specific surface area and in DSSCs owing to high conductivity, respectively.[19] Thus, one of the carbon electrodes of carbon material- based SCs can directly contact with the electrolyte of DSSCs. This concept was demonstrated by Peng et al. who have developed a photocapacitor which adopted aligned multi-walled carbon nanotube (MWCNT) films as electrodes,[20] as illustrated in **figure 2c**. In this configuration, one of the MWCNT electrodes, integrating with a dye-sensitized TiO_2 photoelectrode directly, acted as not only the photoelectrocatalytic electrode for DSSC but also the charge storage component for SC. It differed from the previous back-to-back connection where one of the activated carbon electrodes was coated on one side of a photoelectrocatalytic electrode (such as Pt electrode) of DSSC.[18] The DSSC showed a PCE of 6.1% indicating the MWCNT can replace Pt in catalyzing the redox reactions in DSSC. The device based on the bare MWCNT film with a thickness of 10 μm also had specific capacitance of 48 F g^{-1}, indicating that the energy conversion and charge storage were realized in a single device. Furthermore, with the incorporation of polyaniline (PANI) into MWCNT, the specific capacitance was enhanced. After a photo-charge and galvanostatic discharge cycle, the MWCNT film and MWCNT-PANI composite film-based devices delivered $\eta_{overall}$ of 5.12% and 4.29%, respectively.

Carbon materials have another characteristic of excellent flexibility, therefore the flexible photocapacitors were also developed in recent years.[21-23] Scalia and coworkers reported an innovative device consisting of a TiO_2 nanotube-based DSSC and a graphene-based EDL capacitor integrated into a flexible configuration.[21] They investigated

the photo-charge/discharge characteristics of the integrated device under different illumination conditions and found that the $\eta_{overall}$ increases while lowering the illumination condition (from 1 Sun of 1.02% to 0.3 Sun of 1.46%). The dramatic increase was mainly attributed to the fact that PCE of DSSCs increased under lower light intensity while the energy storage efficiency was not significantly impacted. The additional flexibility test showed the charging behavior was retained with a bending angle of 60° while the charging time slightly increased with a bending angle of 120°. This result indicated the potential applications in practical flexible devices. However, due to a single DSSC in the integrated device that can only give a low open-circuit potential, the charging voltage of SCs was limited. Further investigating for enhancing photo-charging voltage, Lou et al. fabricated a flexible integrated device with an array of three DSSCs connected in series and attained a high charging voltage of 1.8V.[22] The performance of this lightweight high-voltage integrated device was found to be stable under various bending angles.

Besides carbon materials, some conducting polymers, such as PEDOT, poly(vinylidene fluoride) (PVDF), PANI, and polypyrrole (Ppy), were also employed in DS-photocapacitors as charge storage electrodes and delivered nice performance. Thereinto, PEDOT, a widely used conducting polymer, is belong to a derivative of poly(3,4-alkylenedioxythiophene)s (PXDOTs).[24] To see if these derivatives are applicable in photocapacitors, Ho et al. reported one of these derivatives, a poly(3,3-diethyl-3,4-dihydro-2Hthieno-[3,4-b][1,4]dioxepine) (PProDOT-Et_2) as photocapacitor material and compared it with PEDOT.[25] Though PEDOT exhibited slightly better charge–discharge rate, the PProDOT-Et_2 possessed higher electrode specific capacitance with a film thickness of 0.5mm, attributing to the porous nature of synthesized PProDOT-Et_2 film. A photocapacitor composed of a symmetrical supercapacitor based on the suggested thick PProDOT-Et_2 films and a DSSC were fabricated where one of the PProDOT-Et_2 films attached with Pt-electrode of DSSC acted as a common electrode.

This photocapacitor exhibited a photo-charging voltage of 0.75 V, a low specific capacitance of 0.48 F cm^{-2}, and an $\eta_{overall}$ of 0.6%. Such a low specific capacitance was probably due to the mismatch of the electroactive area between polymer and Pt substrate. Employing some electroactive polymers to substitute for the Pt counter electrode could also be effective in the DSSC unit. Deepa et al. employed a Poly(3,4-ethylenedioxypyrrole) (PEDOP)@manganese dioxide (MnO_2) film as the catalytic electrode for the CdS quantum dot (QD)/hibiscus dye co-sensitized solar cell delivering a better PCE of 6.11%,[26] demonstrating that conducting polymer possessed the same effect as Pt. Meanwhile, PEDOP@MnO_2 films were also used as the electrodes for a symmetric supercapacitor. The photocapacitor, in which the PEDOP@MnO_2 based DSSC and SC were integrated on a common current collector, could be charged to 0.72 V under one sun illumination and delivered a specific capacitance of 183 F g^{-1} and a power density of 360 W kg^{-1} at a discharge current density of 1 A g^{-1}.

PVDF and its copolymers are well-known ferroelectric materials for piezoelectric nanogenerators[27] and supercapacitors.[28] In 2011, Jiang et al. used PVDF for the storage of photo-generated electric charges based on a hypothesis that the photoinduced electric field would polarize the ferroelectric material.[29] Later in 2013, they modified the counter electrode of DSSC by PVDF/ZnO nanowire array (ZNWA) nanocomposites to realize a photo-rechargeable charge storage device.[30] From **figure 2d**, the Pt/Au catalytic layer for DSSC and the charge storage interface share the same PVDF surface coated on ZnO nanowires. The PVDF film of 25 nm was used to fabricate the photocapacitors which delivered a specific capacitance of 2.14 C g^{-1}, stable photocurrent output and a $\eta_{overall}$ of 3.7%. However, the charge storage performance relies heavily on the dielectric constant of PVDF. Incorporating highly electroactive sodium dodecyl sulfate (SDS) into PVDF to upgrade the dielectric constant was demonstrated by Das et al., as schematically illustrated in **figure 2e**.[31] Combining this PVDF/SDS film with an inorganic−organic dye film, i.e., ZnO

nanoparticle−eosin Y−poly(vinylpyrrolidone) film, the photocapacitor yielded a high photo-charging voltage of ~1.2V under illumination intensity of ~110 mW/cm^2. A further test of discharging process showed a $\eta_{overall}$ of 3.78% along with a high storage efficiency of ~89% for PVDF/SDS based photocapacitor. In addition, Ppy was a widely used material in photocapacitors. As an example, Gao et al. reported an integrated device consisting of a dye coated TiO_2/PEDOT photo-anode and a ClO_4^- doped Ppy counter electrode.[32] In this configuration, under illumination, the oxidized dye molecule (dye^+) reacted with PEDOT and ClO_4^- , while the photo-generated electrons from the dye flowed from TiO_2 and the external circuit to Ppy and reacted with $Ppy^{x+}\cdot xClO_4^-$ to realize storage of charges. The photo-charging voltage of 0.76V and the $\eta_{overall}$ of ~0.1% were attained, revealing the possibility of using this configuration for direct solar-to-electric energy conversion and storage. Also, Lim and coworkers reported the use of a Ppy/reduced graphene oxide (rGO) electrode as common electrode in a three-electrode DS-photocapacitor.[33] Based on such Ppy/rGO electrode, the PCE of DSSC was 2.4%, and the specific capacitance of the supercapacitor was 308.1 F g^{-1}. Furthermore, an extended lifetime with a retention percentage of 70.9% was obtained after 50 consecutive charge/discharge cycles. However, the associated overall efficiency was not evaluated.

Metal oxides such as titanium oxide,[34-36] ruthenium oxide[37] and nickel oxide[38] as promising pseudocapacitor materials are capable of fast charge propagation in the solid-state and thereby offering high theoretical specific capacitances. Due to the excellent electron-conductivity in DSSC and pseudocapacitive feature, a double-side TiO_2 electrode as common electrode was introduced in three-electrode DS-photocapacitors. Subramanian et al.[34] reported a double-anodized titanium plate (TiO_2–Ti–TiO_2 structure in **figure 2f**) as such a common electrode. On one side of the double-side electrode, the TiO_2-Ti layer acted as the photoanode attaching dye molecules for the DSSC. On the other side of the double-side

electrode, a solid-state zirconia (ZrO_2) dielectric layer was employed to realize charge storage. The photocapacitor based on this TiO_2-ZrO_2 combination achieved capacitance of 140 mF cm^{-2}, and exhibited an obvious voltage increasing under light irradiation, though the overall efficiency was not mentioned. In order to enhance the capacitive performance of TiO_2, Li et al. employed a hydrogen plasma treated double-sided TiO_2 nanotube arrays (TNARs) electrode in photocapacitors.[35] Taking advantage of the simultaneously optimized DSSC and SC sub-devices, the photocapacitor exhibited a $\eta_{overall}$ of 1.64%. Following a similar concept, a flexible photocapacitor based on Ti foil with double-sided TNARs was recently proposed,[36] where CuS networks were used as the catalytic electrode for the DSSC which exhibited remarkable mechanical flexibility, superior transparency, and excellent electronic conductivity, yielding a PCE of 7.73%. This flexible photocapacitor could be charged to 0.64 V in ~30 s under illumination, and supplied electrical energy for 39 s at current density of 8 mA cm^{-2} under dark conditions, delivering a high $\eta_{overall}$ of 6.5%.

To sum up, the presence of common electrodes between DSSCs and SCs is critical for realizing highly integrated photocapacitors. Besides efficient charge transport properties to reduce the internal resistance, the common electrodes serving both SCs and DSSCs needs dual functions of catalysis for DSSCs (similar to Pt electrode) and charge storage for SCs. The carbon materials, conducting polymers and metal oxides are all demonstrated to favorably connect DSSCs and SCs. However, the overall efficiency is still low, which is mainly due to the low PCE of DSSC, thus insufficiently charging the supercapacitors. Therefore, enhancing the performance of DSSCs is imperative. However, there has been no apparent progress on the performance of DSSCs in recent years, whereas the emerging perovskite solar cells and resurgent organic solar cells are gradually becoming substitutes.

2.1.2 Perovskite solar cells

Metal halide perovskite materials with high optical absorption coefficient,[39] long diffusion lengths[40] and high carrier mobility[41] have been regarded as a most promising photovoltaic material. Taking advantage of the bandgap tunability for perovskite materials, the open-circuit voltage V_{oc} for PSCs can reach over 1.0V, which is suitable for high voltage photocapacitors.[42, 43] Over the past several years, PSCs gradually became a competitive solar energy harvesting candidate in photocapacitors.

For PSCs based photocapacitors, the selection of connection materials for PSCs and SCs is crucial for efficient charges transport and thereby high overall device performance. PEDOT and carbon materials not only possess charge storage function in supercapacitors based on EDL capacitance or pseudocapacitance but also are employed in PSCs as carriers transporting layers.[42, 44] Similar to DS-photocapacitors, PEDOT or carbon materials were widely used as common electrode in PSCs based photocapacitors. As an example, a PEDOT-carbon electrode was demonstrated to bridge the supercapacitor part and the perovskite solar cell part.[45] The ClO_4^--doped PEDOT was electrodeposited on the carbon electrode not only as a conductive layer for collecting holes generated form perovskite solar cell, but also as an electrode for a symmetric supercapacitor assembled with another PEDOT-carbon electrode (**figure 3a**). The photo-generated electrons and holes from the excited perovskite can be transferred and electrochemically stored in the PEDOT-carbon cathode and anode. The maximum areal capacitance of 12.8 mF cm^{-2}, a high energy storage efficiency of 73.77% and the maximum overall efficiency of 4.7% during the first cycle were achieved. However, the poor stability of PSCs still restricts future development, especially the degradation of $CH_3NH_3PbI_3$ perovskite in aqueous electrolyte causes difficulty in manufacturing process for photocapacitors.[46] To address this issue, a carbon nanotube composite (CNT) bridge, which was a hydrophobic hole conductor, was used as a common

electrode between $CH_3NH_3PbI_3$ PSC and PANI/CNT SC for effectively preventing the $CH_3NH_3PbI_3$ from degrading (**figure 3b**).[47] Owing to the excellent pseudocapacitive and conductivity of PANI/CNT, the photocapacitor achieved a large specific areal capacitance of 422 mF cm^{-2}, high coulombic efficiency of 95.8%. However, the overall efficiency of 0.77% was still low, which mainly resulted from the mismatch between the MPP of solar cells and the charging voltage of the SCs. During the photo-charging process, the charging current density declined and the voltage of SCs gradually increased to 0.7 V, which was not the MPP **(figure 3c)**. Despite this mismatch issue, PSCs integrated with SCs can still work more efficiently under fluctuating sunlight than individual PSCs, which indicates the SCs can be regarded as a stabilizer for solar cells in the case of integrated photocapacitors.

Recently, a more stable all-inorganic PSC based on cesium lead halide material integrated with a SC was presented. All-inorganic PSCs with higher V_{oc} could enhance the operating voltage and specific capacitance of photocapacitors. Lim et al. firstly fabricated photocapacitors based on $CsPbBr_{3-x}I_x$ PSCs under ambient conditions (relative humidity (RH)> 80%).[48] After comparing a series of $CsPbBr_{3-x}I_x$ perovskite materials, $CsPbBr_{2.9}I_{0.1}$ PSC with high stability was chosen for the photocapacitor application. A asymmetric supercapacitor comprised of PEDOT:PSS-assisted reduced GO/ZnO/Co_3O_4 (RZCo) positive electrode and a Ppy/rGO negative electrode utilizing $LiClO_4$/ acetronitrile as the electrolyte was examined, which delivered a specific areal capacitance of 150 mF cm^{-2} at a current density of 0.1 mA cm^{-2}. The studies of photovoltage and photocurrent responses under light irradiation showed an obvious photo-charging process for this photocapacitor, in which the PEDOT:PSS was a shared intermediate cathode. Similarly, Jin et al. demonstrated an integrated all-inorganic perovskite photocapacitor constructed by combining an $CsPbBr_3$ PSC and an all-inorganic supercapacitor.[49] The $CsPbBr_3$ PSC fabricated by a simple process without the need of glovebox shows high V_{oc} with remarkable stability. The fabricated

supercapacitor consisted of an acidic silica-gel electrolyte layer and two nanocarbon electrodes, in which one of the nanocarbon electrode was shared with the $CsPbBr_3$ PSC. This photocapacitor directly reached a remarkable voltage of ~1.2V charged by a $CsPbBr_3$ PSC without the need of any assistance from galvanostatic-charging. A fast charging process was realized where the supercapacitor unit reached a flat voltage plateau within less than 3s by photo-charging, and then kept this at a stable level without any voltage drop. Also a high $\eta_{overall}$ of 5.1% after first cycle with good stability was realized.

2.1.3 Organic solar cells

Organic solar cells (OSCs), with many attractive features (e.g., flexible, low-cost and easy-fabrication) have been one of the potentially competitive 3rd generation solar cells.[51] Integration of OSCs and SCs is a promising strategy to realize a miniaturized, light weight and portable self-charging device.[52] Srinivasan et al. demonstrated a printable, all solid-state photocapacitor incorporating both an organic solar cell and supercapacitor.[50] The OSC was layer-by-layer fabricated with an ITO layer, a PEDOT:PSS conductor layer, and an active layer blended of poly(3-hexylthiophene) (P3HT) and [6,6]-phenyl-C61-butyric acid methyl ester (PCBM). Then, a patterned Al cathode was deposited on the active layer by thermal evaporation. A single-walled CNT network was deposited on top of the Al as a connection electrode for OSC and CNT symmetric supercapacitor, as depicted in **figure 3d.** The photocapacitor yielded a capacitance of 28 F g^{-1} which was lower compared to an individual SC. This is mainly due to the V_{oc} limitation from the non-optimized OSC, which was insufficient to charge SC up to its maximum capacity. Thus, for further development of such OSC-photocapacitors, several OSCs connected in series could be used to increase photo-charging voltage and realize better voltage matching. Chien et al. demonstrated such an

integrated photocapacitor consisting of a string of series connected OSCs and graphene SCs on a single substrate, using graphene as a common electrode.[53] Eight series-connected OSCs based on P3HT: $PC_{60}BM$ bulk-heterojunction (BHJ) cells provided a V_{oc} of ~5V and an photo-charging voltage of ~4V for the photocapacitor which was suitable for driving red, green, and blue light emitting diodes (LED). Besides, benefiting from easily-fabrication and solution processible features of OSCs, large area OSCs can deliver more energy to store in SCs. A metal-free foldable integrated photocapacitor was processed by laminating a highly conductive PEDOT:PSS film onto a relatively large area P3HT: indene-C_{60} (ICBA) BHJ OSCs.[54] The OSCs achieved a PCE of 3.84% and the PEDOT:PSS based SCs obtained an energy storage efficiency of 58%, resulting in an overall efficiency of 2% for integrated photocapacitors. However, as the OSCs based on P3HT system still have low performance, the corresponding photocapacitors attain inferior overall efficiency. With the recent development of highly efficient organic photovoltaic materials, Arias et al. demonstrated an OSC integrated with a supercapacitor operating under indoor low light intensity with excellent performance, which is meaningful for many electronic products working under indoor conditions.[55] Benefit from the poly[N-9′-heptadecanyl-2,7-carbazole-alt-5,5-(4,7-di-2-thienyl-2′,1′,3′-benzothiadiazole)] (PCDTBT): [6,6]-phenyl-C71-butyric acid methyl ester ($PC_{71}BM$) BHJ OSCs delivering a relatively high PCE of 7.6% under indoor conditions, the OSCs based photocapacitor achieved an $\eta_{overall}$ of 2.92%. Following this trend, Lee and coworkers combined a high-performance BHJ system comprising PTB7-Th electron donor and $PC_{71}BM$ electron acceptor with a polyvinyl alcohol (PVA)/phosphoric acid (H_3PO_4)-based solid-state supercapacitor reaching a higher $\eta_{overall}$ of 5.07%.[56] Very recently, lots of high performance organic photovoltaic materials are springing up, giving a significant increase in PCE.[57] Hence, the overall efficiency of OSCs based photocapacitors may rapidly ascend in the near future.

2.2 SCs employ a photoelectrode

Though the integration of solar cells and supercapacitors is feasible, it still has some disadvantages. When supercapacitors are charged by solar cells, the output electricity from the solar cells may fluctuate because of the unstable sunlight intensity in the actual situation, sequentially causing voltage, current and power mismatch between solar cells and supercapacitors. Moreover, multiple material hetero-interfaces existing in solar cells based photocapacitors are not desirable due to excessive interface impedance. Differing from the utilization of solar cells for photo-charging, employing a photoelectrode with photoactive and pseudocapacitive features simultaneously can also realize photo-charging. Adopting a composite, which couples photosensitive materials with capacitive or pseudocapacitive materials as this dual-function photoelectrode, is an effective approach.[58] For example, attaching photosensitive dye molecules on PEDOT or carbon materials was widely used for dual-function photoelectrodes. Takshi et al. demonstrated a composite film photoelectrode which could convert photons to charges by dye molecule coated PEDOT and at the same time these charges were stored on PEDOT, as shown in **figure 4a**.[59] Using active carbon as the counter electrode, the photocapacitor with a photo-charging open circuit voltage of 430 mV was able to store the charge for more than 10 min in the dark. They also found that the addition of the dye increased the capacitance in the conducting polymer and enhanced the photovoltage in the device. Watanabe et al.[60] prepared a UV light sensitive photoelectrode by electrophoretic deposition of TiO_2 nanoparticles on carbon materials (**figure 4b**), in which charges were generated by TiO_2 under illumination and stored in carbon materials. Assembled with another carbon counter electrode, this photocapacitor can be charged to 100 mV under UV irradiation, attributing to the wide bandgap of TiO_2 which exhibited strong response to UV light.

Except widely used PEDOT or carbon materials, many metal hydroxides or oxides with pseudocapacitive properties may yield a higher capacitance through reversible charge transfer reactions. Concurrently, these materials also show good photoelectric properties.[61, 62] For instance, a photo-charging process was realized based on a TiO_2/transition metal hydroxide ($Ni(OH)_2$) core-shell composite photoelectrode by Fan et al. **(figure 4c)**, where the TiO_2 core harvested photons to generate electrons and holes.[63] The photo-generated electrons were captured by a Pt counter electrode for H_2 evolution and the photo-generated holes were stored in $Ni(OH)_2$ pseudocapacitive materials by oxidation reactions (**figure 4d**). To effectively separate photo-generated electron-hole pairs and realize oxidation of pseudocapacitive materials, a reasonable potential bias of 0.4V was selected which did not cause extra electrochemical reactions. After charging at 0.4 V bias for 300 s under light illumination, the supercapacitor properties were tested by galvanostatic discharge and the corresponding specific capacitance of 482 F g^{-1} at 0.5 A g^{-1} was obtained for a TiO_2/$Ni(OH)_2$ based device. Similarly, TiO_2/NiO and TiO_2/$Co(OH)_2$ based devices presented a specific capacitance of 133 F g^{-1} at 0.5 A g^{-1} and 337 F g^{-1} at 0.5 A g^{-1}, respectively. However, introducing an external potential bias to separate charge carriers did not achieve the goal of direct energy conversion and storage. Thus, Zheng et al. presented a two-photoelectrode supercapacitor building on Fan's work. The TiO_2 nanowire/NiO nanoflakes and the Si nanowire/Pt nanoparticle composites were used as photoanodes and photocathodes, respectively **(figure 4e)**.[64] On the photoanode side, a thin layer of nickel oxide (NiO) nanoflakes was grown on the surface of the TiO_2 nanowires as the hole receptor, which can store holes by oxidation of NiO to nickel oxyhydroxide (NiOOH). On the photocathode side, the photo-generated electrons from Si nanowire can reduce water to H_2 with the assistance of Pt nanoparticle catalyst. As depicted in the energy diagram **(figure 4f)**, this two-photoelectrode supercapacitor fully relied on solar energy for charge carrier separation without external potential bias. A stable open-circuit voltage of ~0.45 V and a high pseudocapacitance of up to ~455 F g^{-1} were obtained from the

first discharge cycle. But, part of the photo-generated holes may also cause water oxidation in aqueous electrolyte, which is harmful for the applications of a supercapacitor. To inhibit water photo-oxidation, the valence band (VB) position of the photoelectric semiconductor and the thickness of $Ni(OH)_2$ shell played significant roles.[65] Compared with TiO_2, the higher VB of Fe_2O_3 with thicker $Ni(OH)_2$ was demonstrated to effectively inhibit water oxidation[66]. After inhibiting water oxidation, the Fe_2O_3@ $Ni(OH)_2$ based photocapacitors exhibited a specific capacitance of 20.6 mF cm^{-2} at a discharge current density of 0.1 mA cm^{-2}.

Some semiconductor materials which simultaneously possess photoelectric and capacitive characteristics have been wildly studied in photocapacitors. Adopting these materials singly as dual-function photoelectrodes is another approach to realize photo-charging. For example, the hexagonal-phase tungsten oxide (h-WO_3) is widely used as photoelectrocatalysis material.[67] Based on the good photoelectrocatalysis and pseudocapacitive performance, employing h-WO_3 as a photoelectrode to realize solar energy conversion and storage is simple and direct. Zhi et al. demonstrated that the capacitance of h-WO_3 based supercapacitor can be increased by 17% under illumination (**figure 5a**).[68] These authors observed that, as the light intensity increases and wavelength decreases, the calculated capacitance increased. The increased capacitance was attributed to the photoexcited electrons from h-WO_3 facilitating pseudocapacitive behavior of h-WO_3.

In addition, cobalt oxides and hydroxides have similar photoelectrocatalysis and capacitive properties to h-WO_3. Sawangphruk et al. observed a significant enhancement in the areal capacitance of a $Co(OH)_2$ SC under light illumination[69]. During the investigation of charge storage performance on a single $Co(OH)_2$ electrode, a symmetric SC and an asymmetric SC revealed a higher areal current and capacitance under illumination than that in dark conditions. As shown in **figure 5b**, the hole (can be regarded as $Co(OH)^{2+}$) and electron

pairs were generated when the $Co(OH)_2$ was excited by blue light and then the $Co(OH)^{2+}$ reacts with the electrolyte to form CoO(OH). This photo-excited process was responsible for the capacitance enhancement. Similarly, very recently, the above authors proposed a Ni-doped Co_3O_4 ($Ni_{0.07}Co_{2.93}O_4$) thin film photoelectrode as positive electrode for supercapacitors which used N-doped reduced graphene oxide aerogel (N-rGO_{AE}) as the negative electrode[70]. As illustrated in **figure 5c**, the energy diagrams explained the photo-charging process. The $Ni_{0.07}Co_{2.93}O_4$ generated electron-hole pairs under illumination and active hole ($Ni_{0.07}Co_{2.93}O_4^+$) reacted with OH^- and H_2O from the KOH electrolyte forming CoO(OH) and NiO(OH). This photocapacitor exhibited an enhanced capacitance which was 1.9-fold higher than that under dark conditions.

The nanometer-sized and interfacial effects between different materials in the composite electrode were beneficial to enhance light absorption and promote the separation of holes-electrons pairs.[67, 71] Based on this viewpoint, Ding et al. designed and fabricated a nanoporous Cu@Cu_2O (NPC@Cu_2O) hybrid array electrode and revealed that the nanoporous Cu promoted the light permeation and enhanced energy storage[72]. The prepared photoelectrode generated electrons and holes under illumination, where the holes oxidized the Cu_2O in the Cu@Cu_2O hybrid to CuO, storing the holes by pseudocapacitance. Simultaneously, the corresponding photo-generated electrons passed through the external circuit to the counter Pt electrode and subsequently reacted with H_2O in aqueous electrolytes to generate H_2. This Cu@Cu_2O photo-assisted supercapacitor delivers 782 F g^{-1} and 314 F g^{-1} at 1 A g^{-1} and 10 A g^{-1}, respectively, thereby achieving 37.9% and 26.6% capacitance increment in comparison to the dark condition.

Compared with the integration of solar cells and SCs, photo-charging a photocapacitor based on photoelectrodes has a simpler device configuration. And the photoelectric conversion and energy storage processes are realized more directly. However, the

photo-rechargeable performance is still at a lower level, and the overall efficiency is barely discussed. Semiconductor materials with outstanding photoelectric activity and capacitive properties simultaneously should be further explored.

2.3 Brief summary

From the above discussions, the feasibility of converting solar energy to electricity and meanwhile storing electric energy as chemical energy for photo-rechargeable SCs has been verified. Based on two types of photo-charging, the photocapacitors exhibited different charging performance. Taken together, photocapacitors based on solar cell charging have remarkable performance compared with photoelectrode charging, which is mainly due to the high PCE of solar cells. Several reported photocapacitors based on solar cells are listed in **Table 1.** However, under prolonged light illumination, the SCs discharge electricity in merely a few minutes or even seconds.[73] Even though the PCE of solar cells has been significantly improved, SCs with fast charge/discharge rates and low energy density cannot satisfy the storage of large amounts of energy. Thereby, the applications in some fields are restricted due to serious energy mismatch between SCs and solar cells. SCs integrated with solar cells may be not suitable as a durable power source for long-time discharge, but as a stabilizer for solar cells under intermittent illumination conditions.

3. Photo-rechargeable static batteries

Nowadays, rechargeable batteries have provided superior energy storage devices for electric vehicles, portable electronics and the internet of things. Different from the SCs,

batteries store electric energy through two processes of internal redox reaction and ionic transfer in electrolytes, which contribute to higher specific energy[74]. In order to distinguish from redox flow batteries, herein, we define the batteries which store electric energy in at least one static solid electrode as static batteries. Similar to photocapacitors, the integration of a PC part and a rechargeable static battery (referred to as photo-batteries) can also realize highly efficient self-charging and storage in one single device.

According to the photo-charging mechanism, photo-rechargeable static batteries can also be divided into two categories of solar cell charging and photoelectrode charging. For the solar cell charging, an obvious difficulty is that the output voltage of single-junction solar cells hardly reaches the charging voltage for most batteries. This is because the redox reaction of the charging process proceeds under a certain voltage for rechargeable batteries, which is different from supercapacitors.[75] Solving the challenge of voltage matching is crucial. On the other hand, charging current (also known as charging rate) also has an impact on the energy storage efficiency of batteries, where excessive low or high charging rate can lead to insufficient energy storage or battery chemistry deterioration.[76] The current matching between solar cells and batteries also should be carefully designed. Moreover, the overall lifetime of the integrated devices is affected by the component with the shortest lifetime. Thus, lifetime matching between solar cells and batteries also needs to be taken into account. For the photoelectrode charging, an integrated photoelectrode in rechargeable batteries realized photo-charging process based on the photoelectrocatalysis effect, which uses semiconductor photoelectrodes to promote the redox reaction occurred on electrode-electrolyte interface under light illumination.[77] The photo-batteries based on photoelectrode charging can straightforwardly convert solar energy to electricity and store electricity in the form of chemical energy,[78] which is similar to the before-mentioned photoelectrode based photocapacitors. Furthermore, the photoelectrocatalysis effect can

alleviate issues of charging overpotential and slow charging rates, which have gradually become the research hotspots in recent years.[79-81] In order to successfully and efficiently charge batteries, the photoelectrode must meet certain criteria. Firstly, it should possess proper band gap to have decent visible light absorption and good carrier transport characteristics. Secondly, the band edge positions should be a trade-off between the conduction band (CB) position of the photoactive semiconductor and the redox reaction to compensate the charge imbalance arising from the cation intercalation.[82] Thirdly, when integrating a photoelectrode into rechargeable batteries, the compatibility and coordination with the redox couple should be considered because various redox couples in rechargeable batteries bring different storage performance.

In this section, we will summarize several mainstream static batteries applied in photo-rechargeable batteries, such as metal ion batteries (e.g., lithium, aluminum or sodium ion battery), metal-air batteries (Li-air battery and Zn-air battery), and metal-sulfide batteries (Li-S battery), etc. In addition, the afore-mentioned two types of charging mechanisms will also be distinguished.

3.1 Metal-ion batteries

3.1.1 Li-ion batteries

Among numerous energy storage devices, Li-ion batteries (LIBs) have been the most mature and large-scale commercialized devices. LIBs are generally composed of an anode (e.g. Li metal, carbon materials or Li_xTiO_2), a Li^+ conducting electrolyte, a separator and a cathode (e.g. $Li(Co/Ni/Mn)O_2$ or $LiFePO_4$ (LFP)). During the charging process, the cathode is oxidized (releasing Li ions), while the anode is reduced (Li ions are inserted).[83] Like the integrated solar cell based photocapacitors, three-electrode photo-batteries were widely

investigated. For example, Wang and co-workers presented an integrated power pack that incorporated a series-wound DSSCs and a LIB.[84] A Ti foil that has double-sided TiO_2 nanotube arrays was used as a common electrode for top DSSC and bottom LIB **(figure 6a)**. The top-side TiO_2 with dye molecules attached (N719 and N749 realized co-sensitization) acted as a photoanode for the DSSC and bottom-side TiO_2 as the anode for $LiCoO_2$ based LIB part. When the top series-connected DSSCs were irradiated, photo-generated electrons from top TiO_2 were injected into the anode of LIB to reduce Li^+. Meanwhile, the $LiCoO_2$ cathode was oxidized releasing electrons to the Pt counter electrode of DSSCs. This integrated device can be charged to about 3 V in about 8 min, with the discharge capacity of about 38.89 μAh under a discharge current of 100 μA with overall efficiency of 0.82%. This inferior overall performance may be attributed to the low-efficiency DSSCs. Though the charging voltage met the requirement, the energy mismatch was serious between DSSCs and LIB due to the small amounts of electric energy converted from solar energy.

Thus, the mismatch between the MPP of solar cells and the optimal charging rate of batteries may cause a low energy conversion and storage efficiency. Many groups have reported multijunction solar cells or the connection of several solar cells in series to obtain high output voltage. A triple-junction thin-film silicon solar cell connecting directly to a LIB was demonstrated by Agbo et al.[85] This triple-junction silicon solar cell delivered a short circuit current density (J_{sc}) of 5.4 mA cm^{-2} and a V_{oc} of 2.21 V which was matched well with the battery characteristics. The overall performance of the integrated devices was discussed in detail based on the voltage, current and capacity curves, as depicted in **figure 6b.** During one photo-charge/discharge cycle, the voltage and current were dynamic with charging time, therefore the overall efficiency was dependent on the state of charge. In region A, the current rapidly increased to the maximum value limited by the J_{sc} of solar cell, and the charging voltage increased to reach a plateau value of 1.9 V. Then the LIB was charged for a while in

region B. The voltage and current were at a steady value appropriately matching the MPP voltage of the solar cell which provided effectively charging of the integrated device. When the charging process was completed, the voltage reached the V_{oc} of solar cell and the current decreased to zero, corresponding to an average overall efficiency of 8.0%. This high overall efficiency was nearly the same as the solar cell efficiency, implying that virtually 100% of the available energy from the solar cell can be transmitted to the battery, which also indicated good voltage and current matching between triple-junction thin-film silicon solar cells and the LIB.

In order to improve the output voltage and power of the whole integrated device and obtain a high area energy density, in other words, to realize good energy matching between LIB and a series solar cells, a tandem battery configuration by connecting two individual $Li_4Ti_5O_{12}$-$LiCoO_2$ based solid-state LIB was employed by Lee and coworkers.[86] They demonstrated a c-Si PC module fabricated by interconnecting 25 units of c-Si mini-cells in series (delivering output voltage of 14.1 V and power of 142.6 mW) for monolithically integrated photo-charging of a solid-state LIB. A current/ voltage tunable c-Si PV module was connected to a printed solid-state bipolar LIB through an Al layer **(figure 6c)**. Attributed to the high energy output of the c-Si PC module and the high-capacity of the tandem solid-state LIB, this Si-LIB photo-battery exhibited rapid charging in less than 2 min with overall efficiency of 7.61% and continuous discharge at a rate of 28C under sunlight illumination.

Perovskite solar cells with their simple preparation process and high PCE were also widely used in photo-batteries in recent years. Dai et al. demonstrated four single $CH_3NH_3PbI_3$ perovskite solar cells connected in series for photo-charging a LIB which was assembled with an LFP cathode and a $Li_4Ti_5O_{12}$ anode.[87] **Figure 6d** shows that the PSCs pack and lithium-ion batteries are connected in parallel. Based on the high performance of

single junction PSCs, for the PSCs pack, a J_{sc} of 4.82 mA cm^{-2}, V_{oc} of 3.84 V, *FF* of 0.68 and PCE of 12.65% were obtained where the voltage was high enough to charge the LIB. The fabricated PSCs based photo-batteries delivered an initial reversible capacity of 140.4 mAh g^{-1} while maintaining a reversible capacity of 111.6 mAh g^{-1} after 10 photo-charge and galvanostatic discharge cycles. And an overall efficiency of 7.80% was realized. Taylor et al. connected two $Cs_{0.05}FA_{0.81}MA_{0.14}PbI_{2.55}Br_{0.45}$ perovskite solar cells in series to charge carbon-coated Li(or Na)$Ti_2(PO_4)_3$ based batteries.[88] The negative electrode of the LIB (or Na ion battery (NIB)) was connected to the photocathode of PSCs while the positive electrode was connected to the photoanode of the PSCs as shown in **figure 6e**. As the PSCs parts delivered a V_{oc} of 2.2V and a high overall PCE of 16.2%, after the first cycle of photo-charging and galvanostatic discharge, the PSCs-LIB and PSCs-NIB obtained a high overall efficiency of 9.25% and 9.3%, respectively. Consequently, this shows that the PSCs exhibit good photo-charging performance not only for photocapacitors but also for batteries. Along with the low-cost manufacturing process and high photovoltaic properties, PSCs possess huge potential in photo-rechargeable ESSs if their stability issues can be overcome.

Photoelectrode charging of a LIB can be realized by the photoelectrocatalysis effect occurring on photoelectrode/electrolyte interfaces, which assists or directly drives redox reaction under light illumination. For instance, photoelectrocatalysis material TiO_2 was integrated into LIBs as a photoelectrode which can reduce charging voltage, consequently reduce external electricity input under illumination.[79] As seen in **figure 7a**, a LIB composed of a Li metal anode and an LFP cathode, in which the LFP cathode was electrochemically connected with TiO_2 photoelectrode by a redox shuttle (M) in aqueous electrolyte. When the TiO_2 photoelectrode harvested the photons, photo-generated holes oxidized the M^{red} to M^{ox}. Subsequently, the M^{ox} diffused to the LFP electrode surface oxidizing LFP to Li^+ and $FePO_4$ and was in turn reduced back to M^{red}. The photo-generated electrons transported to anode

through the external circuit reducing Li^+ to Li metal. From the energy level diagram in **figure 7b**, CB of TiO_2 is lower than $LiFePO_4$/ $FePO_4$ standard potential of 3.45V resulting in a lower charging voltage under illumination. The experimental value of charging voltage was 2.78V, with a voltage reduction of 0.7 V for normal Li/LFP batteries, which matches well with the theoretical prediction. In consequence, the reduced charging voltage indicates that the existing TiO_2 photoelectrode can save input electric energy which was offset by solar energy harvested from TiO_2. Nevertheless, charging LIBs totally by photoelectrocatalysis of the photoelectrode without external electricity input was expected. In view of $LiFePO_4$/ $FePO_4$ standard potential of 3.45V versus Li/Li^+ is very close to the I/I^- potential of 3.1V versus Li/Li^+, which was used in DSSC,[16] photo-catalyzing $LiFePO_4$/ $FePO_4$ redox couple by a dye molecule based on DSSC mechanism is feasible. Zaghib et al. reported LFP nanocrystals mixed with dye molecules as a hybrid photo-cathode.[89] Under illumination, a voltage (versus Li/Li^+) rise of an LFP/dye electrode system was obvious, as shown in **figure 7c**, suggesting photoexcited holes by dye molecules oxidized $LiFePO_4$ to $FePO_4$. Meanwhile, the photo-generated electrons were confirmed to form solid electrolyte interface at the anode via oxygen reduction. During the charge-discharge cycles under light irradiation, a capacity at least two times of the theoretical value of LFP was realized, which was attributed to the continuous photo-charging during the galvanostatic discharge process because of its exposure to light that induced LFP to delithiate. Assembled with a Li metal anode, the overall efficiency for this photo-LIB was estimated to be 0.06-0.08%. Such low efficiency could result from large charge recombination losses at the LFP/dye/electrolyte interface. Thereby, an obvious drawback that poor photo-generated carriers transport efficiency on multiple interfaces for this hybrid electrode-based LIB was exposed.

Another line of thought based on whether lithium ions can display mobility in a photoelectric material upon illumination was proposed. For example, TiO_2 as a good light

absorption semiconductor was demonstrated capable of reversibly hosting Li^+ with an operating potential of 1.75V versus Li/Li^+.[90] Based on the mixed electronic/ionic semiconducting properties of TiO_2, directly using TiO_2 electrode for LIBs can drive the lithium insertion/deinsertion reaction under the photoexcitation.[91] Besides, a lithium rich phase ($Li_{0.5}TiO_2$) is expected to absorb light in the visible range and be a better electronic conductor.[92] Sauvage et al. demonstrated using Li_xTiO_2 nanoparticles can induce a quantitative Li-ion deinsertion reaction by photoexcited holes.[93] **Figure 7d** shows the schematic overview of a half cell, where the Li-ions pre-insertion to form Li_xTiO_2 photoelectrode. Under light illumination, Li_xTiO_2 generated holes to oxidize Ti^{3+} and Li-ions were released out from crystalline lattice. In the dark and illumination conditions, the CV curves exhibited an obvious difference in the position of redox peaks (**figure 7e**), indicating the light affected the kinetics and thermodynamics of Li_xTiO_2 photoelectrode. After the first photoelectrode discharge in dark, a fast light-response was observed and a high potential plateau was preserved regardless of light exposure. In addition, metal halide perovskite materials have also demonstrated the ability of reversibly hosting Li-ion.[94] Combining the outstanding photoelectric feature and Li-ion storage ability of perovskite, Volder et al. demonstrated a photo-charging battery using a 2D-perovskite as photoelectrode and Li-ion storage electrode simultaneously.[95] The 2D $(C_6H_9C_2H_4NH_3)_2PbX_4$ (X is halogen element) perovskite has a very stable layered structure. They first investigated charge-discharge performance of coin cells composed of perovskite electrode and Li metal anode at normal operating regime (non-illumination condition), which showed that the capacities of ~90-100 mAh/g in the first cycle can be offered by lead-iodide perovskite and 410 mAh/g achieved for lead-bromide perovskite. Then, the photo-charging process was investigated and the mechanisms are illustrated in **figure 7f**. This photo-battery displayed a high photo-charged voltage of nearly 3V by perovskite excited under illumination. Despite the demonstrated

feasibility of perovskite photo-batteries in autonomous power conversion and storage, the stability of perovskite materials remains the main concern for its future practical application.

3.1.2 Na-ion batteries

The Na-ion battery is one type of newly-developed rechargeable battery. Similar to Li-ion batteries, energy storage in Na-ion batteries relies on Na^+ migration in electrolyte and redox reaction between anode and cathode, possessing advantages of low toxicity, good reversibility, and high energy density.[96] In general, NaI_3/NaI and Na_2S_4/Na_2S redox couples are widely used in Na-ion batteries.[97] Incorporating a photoelectrocatalysis electrode into a Na-ion battery to realize photo-assisted charging (or photo-charging) is efficient. Similar to photo-assisted LIBs, a TiO_2 photoelectrode has a significant effect on NIBs. Zhou et al. proposed a photo-assisted sodium polysulfide/iodine battery by employing a TiO_2 photoelectrode.[98] As illustrated in **figure 8a**, photo-generated electrons transferred into anolyte by external circuit reduce Na_2S to Na_2S_4, while photoexcited holes into catholyte oxidize NaI into NaI_3. Theoretically, the voltage of sodium polysulfide/iodine batteries is ~1 V based on S_4^{2-}/S^{2-} (2.20V versus Na^+/Na) and I_3^-/I^- (3.22 V versus Na^+/Na). For the photo-assisted batteries, the required theoretical charging voltage can be decreased to 0.07 V because of the potential difference between the redox potential of the S_4^{2-}/S^{2-} couple and CB of the semiconductor TiO_2 (2.27V versus Na^+/Na), as depicted in **figure 8b**, which matched well with the actual charging voltage of 0.08V drawn from the measurements. Significantly, this low charging voltage saves a large of input electric energy. In addition, SnS_2 nanostructured film as photocathode and battery-anode simultaneously was employed in NIBs to simplify the configuration.[99] SnS_2 electrode with a Na-polysulfide solution and super P carbon counter electrode with a Na-iodide solution were separated by a

cation-conductive Nafion-117 membrane. Under light illumination, this device exhibited marked capacity augmentation at various current densities, accompanied by a favorable photo-assisted charge/discharge cycling stability.

3.1.3 Al-ion batteries

LIBs and NIBs still have some limitations of low power density and low energy storage efficiency, which hinder the development of high-power photo-rechargeable ESSs.[2] The emerging Al-ion batteries (AIB) have attracted rising attention thanks to the natural abundance of aluminum, low cost, and high volumetric capacity.[100] Attributing to the fast charging/discharging capability of AIBs, power matching between solar cells and AIBs would be better than that of LIBs and NIBs. Thereby, the utilization of AIBs has the potential to realize high-performance photo-rechargeable ESSs. Very recently, Wang et al. demonstrated an integrated device based on a PSC module and an AIB that were assembled on a bifunctional aluminum electrode without any external circuit (**figure 8c**).[101] The AIBs with fast charge–discharge feature, long cycling stability, and increased safety provided a new avenue to achieve both high power density and large energy density. The PSC module was designed by interconnecting three identical PSCs and the AIB was assembled on the outermost PSC module aluminum electrode. The migration of carriers during photo-charging process was illustrated in **figure 8d**. The photo-generated electrons transferred to the Al anode directly participating in the reduction reaction while the photo-generated holes were injected to hole transport materials flowing to the cathode of AIB. Three connected identical PSCs delivered a high V_{oc} of 3.28V and overall PCE of 18.5%, providing a good match between MPP and charging voltage of AIBs. And the integrated PSC module -AIB exhibited high power density (above 5000 W kg^{-1}), high specific capacity (above 74 mAh g^{-1}), and

robust capacity retention (above 91%) even under the extra-high current density of 5000 mA g^{-1} (less than 1 min photo-charged time). The resulted overall efficiency of 12.04% was among the best in all reported photo-rechargeable batteries.

3.2 Metal-air batteries

3.2.1 Li-air batteries

Li-air batteries have attracted significantly increased attention due to their high theoretical energy density (~3550Wh kg^{-1}), which is several times higher than that of conventional LIBs.[102] Typically, the Li-air battery is composed of a Li metal anode, a porous carbon cathode (acting as an oxygen host) and a Li^+ conducting electrolyte. During the discharge process, Li_2O_2 is formed on the cathode surface by the reduction reaction of O_2, which is reversible in the charging process. The basic discharge/charge reaction can be written as: $2Li^+ + O_2 + 2e^- \leftrightarrow 2Li_2O_2$. Theoretically, the formation of Li_2O_2 during discharging process is at a potential of around 2.7V versus Li/Li^+.[103] Unfortunately, poor conducting and insoluble properties of bulk Li_2O_2 lead to a high charging overpotential. There are two main strategies for reducing the overpotential, i.e. introducing solid catalysts and dissolving redox mediators (M^{red}/M^{ox}).[104] However, the effect from reduction of overpotential is still unsatisfying. The integration of PC part into Li-air battery can address overpotential effectively. In 2014, Wu et al. proposed the use of a triiodide/iodide redox mediators to couple a built-in dye-sensitized TiO_2 photoelectrode with the oxygen electrode for the photo-assisted charging of a Li-air battery.[105] As shown in **figure 9a**, this photo-assisted battery consisted of a Li metal anode, a carbon layer as oxygen electrode and a dye-sensitized TiO_2 photoelectrode. The triiodide/iodide redox mediators (M^{red}/M^{ox}) were sandwiched between photoelectrode and oxygen electrode. The energy level and

photo-assisted charging reaction are illustrated in **figure 9b**. In brief, under illumination, dye generated electrons injected into TiO_2 reducing Li^+ at anode, and the dye translated to dye^+ oxidizing M^{red} to M^{ox}. Subsequently, M^{ox} diffusing to carbon layer oxidized the Li_2O_2 to O_2. In consequence, the photo-charging compensated charging voltage resulting in a lower overpotential, where the charging voltage was reduced to 2.72V from 2.96V. Zhou and coworkers have also made a great effort for photo-assisted Li-air batteries.[106] They integrated g-C_3N_4 photoelectrocatalytic electrode into Li-air batteries to address the issue of high overpotential, wherein the g-C_3N_4 simultaneously acted as both photoelectrode and oxygen electrode, with the photo-assisted batteries achieving an ultralow charging voltage of 1.9V. Considering the deleterious effects of triiodide/iodide redox mediators, they later presented a direct unmediated oxidization reaction of solid Li_2O_2 by photo-generated holes from g-C_3N_4.[107] As depicted in **figure 9c,** the photo-assisted charge voltage equals to the energy difference between the redox potential of the Li^+/Li couple and CB of g-C_3N_4 (1.7 V). Compensated by this photo-charging voltage, the charging voltage of 1.96V was achieved. Although the overpotential was decreased, the problem of electrolyte decomposition under illumination turned up, which accounts for the poor cycling stability. To address this issue, Zhou et al. introduced a stable super-concentrated electrolyte system composed of specific contacted-ion-pairs structure against the illumination-induced decomposition.[108] More importantly, a hybrid charging strategy was rationally designed with an integrated typical and photoelectrocatalysis-involved charging process, in which the highly polarized charging stage is rationally substituted by the photo-assisted Li_2O_2-scavenging process (**figure 9d**).

3.2.2 Zn-air battery

Considering the environmental friendliness and earth-abundance of elemental, Zn, the Zn-air battery was proposed as a promising option for large-scale energy storage with outstanding features such as ultrahigh theoretical energy density (1086 Wh Kg^{-1}), great safety, and low cost.[109] However, the sluggish oxygen reduction and evolution reactions (ORR/OER) at air electrodes have been restrictions for high performance Zn-air batteries. The actual output voltage is always less than theoretical value (about 1.6 V) due to the huge polarization of the ORR, which results in a lower energy density.[110] Except for using electrocatalyst, photoinduced ORR can significantly increase the output voltage, which has been demonstrated by Li et al.[111] A polymer semiconductor polytrithiophene (pTTh) as the cathode, simultaneously as the photoelectrode, was reported for direct conversion of solar energy into electric energy. Under illumination, photoelectrons were generated in the CB of pTTh and transferred to O_2 for its reduction to the intermediate HO_2^-, which is unstable and spontaneously disproportionated to OH^-, then oxidation of Zn to ZnO was led by accepting holes in the VB of pTTh, as illustrated in **figure 10a.** Due to the photoinduced ORR, the discharge voltage was significantly increased to 1.78 V which surpassed the thermodynamic limit of a conventional Zn-air battery, and could maintain during several discharge-charge cycles. This high discharge voltage corresponded to an energy density increase of 29.0% as compared to 1.38 V for a Zn-air battery with state-of-the-art electrocatalyst of Pt supported on carbon black (Pt/C). In consequence, integrating a photoelectrode to photo-induced ORR is a promising strategy for high performance Zn-air batteries. However, in the opposite direction for the OER, the pTTh was not effective to promote charging process. Very recently, Hu et al. using $BiVO_4$ and α-Fe_2O_3 photoelectrodes as air electrode realized a record-low charge voltage of ~1.20 and ~1.43 V, respectively.[80] The device configuration with working mechanism of photoelectrode-promoted Zn-air battery is depicted in **figure**

10b. During the charging process under light illumination, the holes generated from photoelectrode migrated to the photoelectrode surface to oxidize water to oxygen. Based on the principle that the VB potential of photoelectrodes lie higher than the O_2/OH^- couple potential,[112] $BiVO_4$ and α-Fe_2O_3 photoelectrodes with suitable energy band structure were selected to facilitate the OER reaction, as depicted in **figure10c**. Compared with the $BiVO_4$ of which the severe photocorrosion resulted inferior cycling stability, α-Fe_2O_3 exhibited more promising potential as stable and efficient air photoelectrode.

This integrated strategy opened a new pathway for the utilization of solar energy. At present, it has merely realized photo-assisted charging/discharging of Zn-air batteries. If an integrated photoelectrode can further drive the entire photo-charging process, the high-performance self-charging Zn-air batterie will have great application potential.

3.3 Li-iodine battery

Li-iodine battery consists of an anode which can reversibly host Li^+ (e.g. Li metal and some compound) and an iodine-based catholyte (I_3^-/I^- redox couple), which deliver high capacity, coulombic efficiency, and excellent cycling stability.[113] In this battery, fundamental electrochemical reaction can be described as: $2Li + I_3^- \leftrightarrow 2Li^+ + 3I^-$. Particularly, aqueous iodine-based catholyte is favorable to link with photoelectrode for the efficient photo-charging process. The I_3^-/I^- redox couple were widely used in DSSC and redox reaction was driven by a dye-sensitized photoelectrode. Thus, incorporating a sensitizer into photoelectrode to photo-catalyze I_3^-/I^- redox reaction for photo-rechargeable Li-iodine batteries was a generally adopted strategy. Wu and coworkers demonstrated a photo-assisted Li-I battery by incorporating a dye-sensitized TiO_2 photoelectrode.[114] Assisted by solar energy, this Li-I battery can be charged at a charging voltage of 2.9V, which is much lower

than that of conventional Li-iodine battery (3.6V), indicating energy savings of up to 20% ((3.6V-2.9V)/3.60 V×100% = 19%). As illustrated in **figure 11a**, upon illumination, dye molecules are photoexcited and inject electrons into the CB of TiO_2, then the oxidation of I^- to I_3^- takes place by regenerating oxidized dye molecules. Meanwhile, Li^+ ions pass through the ceramic membrane and are reduced to metallic Li on the anode side. The photo-assisted charging voltage is attributed to the photo-generated electrons and holes participating in the Li/Li^+ and I_3^-/I^- redox reaction, with this voltage equivalent to the energy difference between the Li^+/Li redox potential and the E_f of electrons in the TiO_2. In addition, Wei et al. also designed a photo-rechargeable Li-I battery using a dye-sensitized TiO_2 photoelectrode, in which the charging process was completely accomplished by the photoelectrode.[115] More importantly, the WO_3 was chosen to substitute metallic Li as the anode material for Li ion insertion/extraction. As depicted in **figure 11b**, Li ions intercalated in WO_3 convert into Li_xWO_3, and meanwhile, light-induced holes (dye molecule radical cation dye^+) are neutralized by I^- producing I_3^-. A remarkable feature of this photo-rechargeable battery is that upon the exposure to the low light intensity of only 7.5 mW cm^{-2} for 10 min, the first specific discharge capacities of WO_3 nano-film can reach 40.6 mAh g^{-1}. This good performance under low light intensity can be attributed to the strong photoelectric response of the adopted dye molecules. Considering that the CB edge of CdS at roughly 2.5 V vs. Li^+/Li aligns favorably with the CB of WO_3 located at about 3 V vs. Li^+/Li,[116] instead of incorporating a dye into WO_3-TiO_2 electrode, Demopoulo and coworkers selected the CdS as photo-absorbing materials, as shown in **figure 11c**.[117] The photo-excitation and lithium insertion/extraction simultaneously occurred on this single CdS-WO_3-TiO_2 electrode making a simple device configuration. The discharge capacity reached its maximum of 19.5 mAh g^{-1} when the photoelectrochemical cell was photo-charged for 5 h.

Very recently, solid-state electrolyte rechargeable batteries attracted enormous research attention due to its safety. Gao et al. proposed a quasi-solid-state photo-rechargeable battery with poly(ethylene oxide) (PEO) electrolyte as the cathode and an anode electrolyte.[118] Soluble LiI and 9,10-anthraquinone (AQ) were used as cathode and anode respectively (**figure 11d**). During the photo-charging process, I^- was oxidized to I_3^- by dye^+ in catholyte and Li^+ was reduced and inserted into AQ forming Li_x(AQ). The photo-charging voltage of this battery jumped rapidly to 0.65V under light irradiation and then gradually increased to 0.74V. When discharged at 4 mA g^{-1}, a slower discharging process occurred for this quasi-solid-state battery compared with liquid electrolyte battery, indicating a slow activation process and diffusion of lithium ions in PEO electrolyte. And the corresponding discharge capacity of 0.9 mAh g^{-1} was lower than that in liquid electrolyte battery. Even so, the working stability of this quasi-solid-state electrolyte was better than that of liquid electrolyte. Though it was still with low capacity and overall efficiency of less than 0.3%, the concept of quasi-solid-state solar rechargeable battery was demonstrated to feasible.

Direct integration of a semiconductor photoelectrode with photoelectrocatalysis instead of dye-sensitized electrode into Li-I batteries could simplify the device configuration. As an example, hematite (α-Fe_2O_3) has been known to be a promising photoelectrode in photoelectrochemical owing to its suitable optical band gap (1.9-2.2 eV) allowing for the absorption of visible light, excellent chemical stability in neutral and basic aqueous media, as well as abundance, low-cost, and environmental inertness.[119] Byon et al. reported a concept of employing α-Fe_2O_3 as photoelectrode to photo-charge Li-I batteries (**figure 11e**).[120] Promotion of I^- oxidation and decrease of charging voltage suggested that α-Fe_2O_3 photoelectrode optimized the charging process. This Li-I battery exhibited an electric energy storage efficiency around 95.4% with a charging voltage of ~3.43 V, showing greater power and energy densities and cycle stability.

3.4 Li–Sulfur battery

Lithium-sulfur batteries (LSB) with high energy density (sulfur is expected to deliver a specific capacity of 1675 Ah Kg^{-1} and an energy density of 2600 Wh Kg^{-1}) and power density are expected to meet the increased energy storage requirement.[121] LSBs have a suitable charge voltage plateau near 2.4 V and a cut-off charge voltage at about 2.8 V,[122] which is easy to match the photovoltaic devices. Gao et al. assembled a serially connected PSCs module (three PSC units were connected in series) with a high V_{oc} up to 2.8 V and the MPP near 2.4 V, which was appropriate for charging an LSB as requested by voltage matching principle.[123] As shown in **figure 11f**, the photo-generated holes were collected by the dense carbon layer oxidizing polysulfde anions into the elemental sulfur on porous carbon layer. Meanwhile, the photo-generated electrons reduced Li^+ to Li metal flowing from TiO_2 and external circuit. Owing to good matching between solar cells module and LSB, the compact structure led to an overall efficiency of 5.14%. And the LSB can retain high specific capacity up to 762.4 mAh g^{-1} under ultrafast photo-charging rate within 30min. However, there are few reports focused on photo-rechargeable LSBs at present, which probably due to a bad cycling stability of LSBs.[124] Herein, we present an imagine that alleviate side reactions of producing polysulphides accordingly improve cycling stability through photoelectrocatalysis effect of a photoelectrode, which is similar to before mentioned photoelectrode assisting charging process. Best to our knowledge, there have been no reports on photo-assisted LSBs to solve issues of side reaction. If the photo-assist method works well, LSBs field will face a new opportunity of growth.

3.5 Brief summary

The photo-rechargeable static batteries are regarded as the most promising photo-rechargeable ESS due to the combination of high PCE of PC units and high efficiency of storing electricity in batteries. For a high-performance battery, especially for commercialized Li-ion battery, integrating it with solar cells or photoelectrodes to realize self-charging demonstrates huge potential for portable devices application. In addition, integrating photoelectrodes into batteries has taken good effect on catalyzing redox reaction. Several of photo-chargeable static batteries are compared in **Table 2.** However, the overall efficiency of integrated devices is still at a low level, for which the match of the performance parameters between PC unit and batteries play a crucial role. For voltage matching, it should rationally connect several solar cells in series or select photoelectrodes with suitable band edge to drive redox reaction.[85, 87] And for current density, the area of PC units and batteries should be optimized.[86] The Energy matching between PC units and batteries is crucial to overall efficiency, where too little converted energy by PC units or too low capacity of batteries goes against performance improvement. In addition, when photo-charging proceed with the integrated solar cells, the voltage of battery is gradually increasing. The fact that solar cell is working under reverse bias voltage should be considered. Under reverse bias voltage, the internal energy level structure of photoelectric materials could be changed. However, previous reports barely discussed this issue.

4. Photo-rechargeable redox flow batteries

Conventional static batteries in which the energy store in at least one static solid electrode material cannot satisfy the requirement of large-scale energy storage, resulting from the fact that high storage capacity always relies on larger-volumes cells. Redox flow battery (RFB), wherein the energy is stored in fluid electrolytes and storage capacity is determined

by the fluid redox species and the electrolyte volume and concentration, is capable of large-scale energy storage and has recently attracted considerable research interest.[125] The RFBs are composed of an electrochemical cell and two separate tanks where liquid electrolytes (catholyte and anolyte) containing redox species are stored. The electrochemical cell consists of two chambers in which redox reactions of two liquid redox couples occur independently and are separated by an ion exchange membrane. And two electrodes are electrically connected with liquid redox couples to collect and deliver current.[126] The electrochemical cell can be regarded as a photoelectrochemical cell when integrated with a PC unit, in which the photo-charging process is realized by photoelectrodes driving the electrolyte redox reaction, as depicted in **figure 12a**. The discharged redox couples in catholyte and anolyte respectively flowing into photoelectrochemical cell will be charged under illumination and then flow out to discharge. In order to drive the charging reactions of RFB without additional power source under light, a principle that light harvesting part must generate higher potential than that of redox reaction should be followed. For semiconductor photoelectrode, the VB at a sufficiently positive potential can produce holes to oxidize the redox couple in the catholyte, whilst the CB at a sufficiently negative potential can produce electrons to reduce the redox couple in the anolyte. Based on this principle, considering that the RFB has two individual redox chambers, photo-charging an RFB could be achieved on two configurations: single side and dual-side photo-charging, as illustrated in **figure 12b and c**.

4.1 Single side photo-charging

Single side photo-charging configuration as a simple form offers advantages of potential scalability and low-cost cell design. Under light irradiation, a single photoelectrode generates

holes to oxidize catholyte at the photoelectrode-catholyte interface, or generates electrons to reduce anolyte at the photoelectrode-anolyte interface. Theoretically, in order to efficiently drive a redox reaction, a single semiconductor photoelectrode needs a wide bandgap material with lower VB below oxidation potential and higher CB over reduction potential.

Considering the diversity of redox couples for RFB, the selection of a semiconductor photoelectrode with suitable bandgap matching with the redox potential is important. Conventional vanadium RFB is the most intensively investigated system with standard cell potential of 1.26V.[127] Thus, the selection of a photoelectrode to drive redox reaction need bandgap greater than 1.26 eV. For example, CdS, WoO_3 and TiO_2 et al. with suitable wide-bandgap of over 2.0 eV can directly charge pairs of V^{3+}/VO^{2+}.[128, 129] However, vanadium based redox couples with high redox potential cause many single photoelectrode to have difficulty to unbiased photo-charging. Besides V^{3+}/VO^{2+} redox couples, other redox couples with a matched photoelectrode are feasible. Mendes et al. reported a photo-rechargeable RFB with an aqueous solution of ferrocyanide ($Fe(CN)_6^{4-}/Fe(CN)_6^{3-}$), and with NaOH as catholyte and an aqueous anthraquinone-2,7-disulphonate (AQDS) and NaOH solution as anolyte, yielding a standard cell potential of 0.74 V.[130] A hematite photoanode (with bandgap of 1.9eV) immersed in catholyte realized unbiased photoelectrochemical charging under illumination attributing to the VB and CB positions of hematite cover the energy levels of the redox couples. However, the battery can only be charged without external bias up to about 10% state-of-charge, where a fully charged and discharged battery corresponds to state-of-charge of 100% and 0%, indicating that the photovoltage (out-put voltage of photoelectrode under illumination) was lower than expected from the band position considerations. This is mainly because the photo-generated electrons reducing ferricyanide instead of AQDS, as illustrated in **figure 13a**. Hence, an annealing treatment was employed and a layer of a conductive polyaniline polymer was grown on the hematite surface

to improved performance in terms of ferrocyanide oxidation photovoltage. However, the overall efficiency of only 0.08% was achieved, thus the more efforts on energy conversion efficiency and photoelectrode/electrolyte interface should be paid. Very recently, they proposed iodide/iodine (I^-/I_2) redox couple on the catholyte side to replace $Fe(CN)_6^{4-}/Fe(CN)_6^{3-}$ redox couple,[131] exhibiting a stable battery cycling with a cell voltage of ~0.8 V, a high coulombic efficiency of 99.2% and a peak power density of 0.22 W cm^{-2}. Furthermore, a tandem photoelectrode was fabricated by hematite photoelectrode connected in series with DSSCs providing a photovoltage of 1.6 V, which realized complete unbiased photo-charging of the I^-/I_2-AQDS based RFB. The tandem-configuration photoelectrode showed its superiority of high photovoltage to efficiently photo-charge the RFB.

In fact, the attempts of tandem-configuration photoelectrode have been reported previously before.[128, 132] For example, Jin et al presented a tandem photoelectrode with high efficiency and high photovoltage that was properly matched with high-cell-voltage RFB.[132] They chose organic redox couples 4-hydroxy-2,2,6,6-tetramethylpiperidin-1-oxyl (4-OH-TEMPO) and methyl viologen as the anolyte and the catholyte, respectively, for the integrated RFB device, delivering a high voltage of 1.25V. A high-photovoltage triple-junction III-V tandem photoelectrode that consists of an InGaP top cell (Eg = 1.85 eV), a GaAs middle cell (Eg = 1.42 eV), and a Ge bottom cell (Eg = 0.67 eV) was utilized as shown in **figure 13b**. Moreover, this triple-junction cell can even work as a single photovoltaic cell providing a high photovoltage of 2.4V, which is beneficial for high-voltage RFB. Over ten cycles, the integrated photo-RFB device achieved a stable overall efficiency with an average value of 14.1%.

The Br_3^-/Br^- and I_3^-/I^- redox couples in catholyte and anolyte, respectively, with rapid redox kinetics have also been widely used in RFB to store and deliver energy with high energy storage capacity.[133] For photoelectrochemical charging a Br_3^-/Br^- and I_3^-/I^- based

RFB, Yu et al. summarized several photoelectrode materials with suitable bandgap that can catalyze the redox reaction of Br_3^-/Br^- and I_3^-/I^- redox couples, as indicated in **figure 13c**.[134] For obtaining high conversion efficiency and high durability of photoelectrodes, a WO_3-decorated $BiVO_4$ photoanode with suitable energy level was presented, which has been demonstrated to possess high light harvesting efficiency and high charge separation efficiency.[135] Using this composite electrode, a single-photoelectrode-driven RFB reached an overall efficiency of 1.25%.

In addition, the dye-sensitized photoelectrode can also be integrated into photo-rechargeable RFB along with a typical used I_3^-/I^- redox couple in catholyte.[136, 137] Generally, under illumination, dye molecules get excited and generate holes (dye^+) to oxidize I^- ions to I_3^- ions at the photoelectrode-liquid interface. Meanwhile, photo-generated electrons are injected into the CB of the semiconductor photoanode, which then flow through the external circuit to reduce anolyte. Like semiconductor photoelectrode, the energy level position of the dye molecules should match the energy difference between the I_3^-/I^- in catholyte and the other redox couple in anolyte. Yang et al. selected redox-active I_3^-/I^- and $[Fe(C_{10}H_{15})_2]^+/Fe(C_{10}H_{15})_2$ (denoted as $DMFc^+$/DMFc) as two redox couples.[136] The redox potential of the I_3^-/I^- couple was approximately 0.7 V more positive than that of the $DMFc^+$/DMFc couple and 0.15 V lower than that of dye Z709, indicating the effectiveness of photo-charging RFB.

4.2 Dual-side photo-charging

Dual-side photo-charging configuration employs a photoelectrode at each side of RFB. As depicted in figure 12c, at the cathode side, the photoelectrode needs lower VB to generate holes oxidizing the catholyte, and at the anode side, the other photoelectrode needs higher CB

to generate electrons reducing the anolyte. It is different from the single side configuration which demands both suitable VB and CB in a single photoelectrode. Thereby, dual sides photo-charging configuration lowers the requirement of the tuning of semiconductor bandgap, indicating narrow bandgap semiconductors allowing for efficient utilization of solar energy can be explored for photo-rechargeable RFB.

For instance, based on p-type and n-type Si formed by metal elements doping, the fabricated Si p-n junction cell (n^+ p or p^+ n) can efficiently separate electron-hole pairs and induce a befitting photovoltage to drive RFB charged. Li et al. reported an efficient photo-rechargeable RFB based on a dual-Si photoelectrochemical cell (**figure 14a**),[138] in which the AQDS/$AQDSH_2$ and Br_3^- /Br^- were used as active redox couples. Under illumination, the n-Si oxidized the Br^- to Br_3^- and p-Si reduced AQDS/$AQDSH_2$, giving a self-charged cell voltage of 0.8 V and the discharge capacity of 730 mAh L^{-1} after photo-charging for 2 h. The final overall efficiency of the dual-Si photo-rechargeable RFB exceeds 3.0%, which can be attributed to the outstanding light harvesting properties of silicon, active surface cocatalysts, as well as rapid kinetics of redox couples. Jin et al. also reported a quinone redox couples (AQDS/$AQDSH_2$ and BQDS/$BQDSH_2$) based RFB photo-charged by dual Si photoelectrode, depicted in **figure 14b**.[139] The redox potentials for AQDS and BQDS redox couples are 0.21 V and 0.89 V, respectively. The used Si heterojunction photoelectrodes (p^+ n n^+-Si/Ti/TiO_2/Pt photocathode and n^+ n p^+-Si/Ti/TiO_2/Pt photoanode, as illustrated in **figure 14c**) generated voltage of about 1V, which is high enough to drive the charging process. Nevertheless, the used BQDS redox couple is chemically or electrochemically unstable for long-term energy storage, and the photocorrosion of semiconductor photoelectrodes in aqueous is very serious.[140] Regarding the device lifetime, Jin et al. developed an unprecedented stable photo-RFB with continuous cycling performance over 200h based on a neutral pH aqueous electrolytes of

bis((3-trimethylammonio)propyl)-ferrocene dichloride (BTMAP-Fc) and bis(3-trimethylammonio)propyl viologen tetrachloride (BTMAP-Vi) and well-protected silicon photoelectrodes.[141] The two Si photoelectrodes were both fabricated by forming internal solid-state p-n junction: n^+ n p^+-Si as photoanode and p^+ n n^+-Si as photocathode. This photo-RFB maintained a high overall efficiency during the 200h cycling test with an average efficiency of 5.4%, which was a record stable efficiency in comparison with previously reported photo-RFB systems. However, the demand for higher photo-charging voltage is still a critical challenge for narrow-bandgap photoelectrodes. Wang et al. demonstrated a high photovoltage exceeding 1.4 V obtained from Ta_3N_5 nanotubes photoanode and GaN nanowire/Si photocathode to photo-charge 2,6-DHAQ (2,6-dihydroxyanthraquinone)/$Fe(CN)_6^{4-}$ liquid redox systems (cell voltage 1.2 V).[142] As shown in **figure 14d**, the high photovoltage was enabled by more positive VB edge position of Ta_3N_5 and more negative CB edge position of GaN.

4.3 Brief summary

Comparing the above-mentioned two configurations, the obvious superiority for single side photo-rechargeable RFBs is its simpler device configuration, which brings lower manufacturing cost. However, the redox reactions driven by a single photoelectrode require appropriate bandgap position and values of the photoelectrode. Generally, the wide bandgap is needed to provide sufficient driving forces for the redox reactions. However, the use of the spectrum is limited for wide-bandgap photoelectrode, resulting in a low overall efficiency. On the contrary, dual side photo-rechargeable RFBs need two photoelectrodes with suitable VB and CB, respectively, which can lower the requirements for photoelectrode materials. Thus, many more candidates with narrower bandgap and excellent photovoltaic performance

could be selected. Consequently, the overall efficiency of dual side configuration is generally higher than that of single side configuration.

One most notable advantage of integrating PC units and RFBs is converting and storing solar energy at a large scale and in real time, which is mainly attributed to the energy storage in flowing electrolyte. But, to realize efficient photo-charging, options of redox electrolytes and semiconductors are still facing challenges, which need good energy level matching. In-depth fundamental research for semiconductor-electrolyte interface should be prioritized. Redox couple electrolyte systems with high solubility, fast kinetics, and low ionic resistance should also be paid more attention. It is expected that the photo-rechargeable RFBs could be well positioned in the large-scale energy storage market, and a photovoltaic energy storage station is predictable if the further breakthrough is made in addressing these challenges.

5. Discussion

5.1 Current state of applications

Despite the enormous number of reports on photo-rechargeable ESSs are focused on materials and basic device performance rather than practical applications, there are some good case studies in the application sector. A representative form is the integrated energy wire,[9, 11, 143, 144] which is beneficial to be applied in wearable devices. Some generally integrated energy wires can be seen in **figure15a and b.** These energy wires have a common characteristic of a coaxial PC part and EES part, which can realize energy conversion and storage simultaneously. Besides, Peng et al. fabricated an integrated energy wire with a core-sheath structure, in which the PC part at the sheath and the lithium-ion storage part at the core (as depicted in **figure 16a**).[145] Compared to the general structure, the core-sheath

structure realized more energy conversion and storage at the same length. This integrated energy wire was lightweight and flexible, thus can be readily used in clothes. They demonstrated a smart glove based on integrated energy wire to power two light emitting diodes connected in parallel, as shown in **figure 16b and c**. Upon illumination, the energy wire converted light to electricity which was stored in the lithium-ion storage part. In dark conditions, the stored electrochemical energy was converted to electric energy to light up the light emitting diodes.

There are only a few reports on practical applications indicating a huge exploratory space for integrated photo-rechargeable ESSs. For future direction, simplifying the manufacturing process, reducing the costs and improve overall efficiency are the key points.

5.2 Parameters matching and comparison

Among three types of integrated photo-rechargeable ESS, a relatively large amount of researches has been conducted directed at photo-rechargeable SCs, particularly for individual solar cell charged SCs, probably resulting from this being the simplest device configuration and energy storage mechanism of SCs. However, the energy and power between SCs and solar cells suffer from serious mismatch. Thus, SCs with fast charge/discharge rates and low energy density are more suitable for short-term energy storage. Photo-rechargeable SCs would be mainly designed to provide a buffer and make the power output from solar cells more stable. In comparison, photo-rechargeable static batteries have great potential as self-charging devices for real applications in our daily life. Storage of electrochemistry energy in a solid material allows static batteries to possess both higher energy density and portability. Careful optimization of the parameter matching between solar cells and batteries could lead to a higher overall efficiency. In addition, whether photocapacitors or

photo-batteries, choosing a photoelectrode with good photoelectrocatalysis activity and charge storage ability can not only simplify the device configuration but also facilitate the photo-charging process. Also for photo-rechargeable RFBs, using photoelectrodes to build a photoelectrochemical cell is the main approach to drive photo-charging. Integrating photoelectrodes into ESSs is a simple and straightforward strategy, whereas, due to the low efficiency at present, more efforts on the fundamental research of semiconductor-electrolyte interfacial chemistry should be devoted in future development. The properties of different types of integrated photo-rechargeable ESS are compared and listed in **Table 3.**

Another noteworthy parameter is the lifetime matching between PC units and ESSs, which is of great significance in practical application. Take the case of static batteries which have limited cycle life, when it is integrated with a long-lifetime silicon solar cell, the lifetime of the whole integrated device is restricted by battery part, in which the silicon solar cell is wasted. In this aspect, some highly efficient solar cells with low cost and relatively short lifetime (such as PSCs and OSCs) could be more appropriate for static batteries,[87] while long-lifetime solar cells (silicon solar cells and inorganic compound solar cells) may play a greater role in high-capacity and long-lifetime photo-rechargeable RFBs.[132, 138] In brief, for obtaining a more rational design of photo-rechargeable ESSs, and maximum economic benefit, there has to be a good lifetime matching between PC units and ESSs.

5.3 Unit-time overall efficiency

In the reported literatures, the reported overall efficiency usually takes into account the input energy from light which is just enough to charge ESSs to a certain voltage. However, the input energy in actual situations is constant. In other words, for photo-rechargeable EESs, even if the energy storage part has reached saturation, the PC part still converts input solar

energy to electricity and is able to charge the energy storage part. Thus, the reported efficiency is insufficient to evaluate performance comprehensively. Considering the capability is different for various ESSs, meanwhile, the different PC devices proceed at different photo-charging rates. We think that the introduction of time into the overall efficiency determination is reasonable. To facilitate understanding, we make an assumption that two different photo-rechargeable ESSs have the same overall efficiency, but one is low-capacity with quick photo-charging and another is high-capacity with slow photo-charging. Under sunlight illumination, two photo-rechargeable ESSs obtain the same solar energy within the same time interval, but the one with slow photo-charging will output more energy attributing to its high capacity. Consequently, we propose the use of unit-time overall efficiency which can be obtained from the following formula (2):

$$\eta_{unit-time\ overall} = \frac{E_{output}}{E_{light} \times t} \times 100\% \quad (2)$$

where the t is illumination time. For example, for overall efficiency evaluation of a daily-used portable integrated device, the illumination time of one or five hours as a unit under one sun condition (AM 1.5 and 100 mW cm^{-2}) is suggested. This formula emphasizes time, which is different from the formula (1). The unit-time overall efficiency not only reflects the ability of energy conversion and storage within a certain illumination time frame, but also highlights the power matching and energy matching between PC units and ESSs. Based on this concept, the performance of photocapacitors and photo-batteries can be clearly differentiated. For example, if using the same PC devices to constantly charge SCs and batteries within the same illumination duration, the unit-time overall efficiency of photocapacitors will be obviously lower than that of photo-batteries, which is caused by the generally lower capacity of SCs. Moreover, the photo-batteries may show higher unit-time overall efficiency, indicating less waste of input energy.

6. Outlook

Currently, most research and development for photo-rechargeable ESSs are still in an early experimental stage, presenting numerous problems and challenges that need to be addressed such as lack of fundamental insights, complex manufacturing process, and poor device performance. Thereby, we make some suggestions for the future development of photo-rechargeable ESSs.

1) More in-depth theoretical research focusing on parameter matching (i.e., voltage matching, current matching, energy matching, power matching, and lifetime matching) between the PC unit and energy storage part should be the first priority. To achieve high performance on integrated devices, whether solar cells or photoelectrodes, the parameter matching between PC units and electric energy storage units is crucial. Simulation or modeling studies could be beneficial to better predict the performance of these systems.

2) High efficiency photoelectric conversion and energy storage materials play an important role in photo-rechargeable ESSs to achieve outstanding performance. As mentioned previously, perovskite materials as the alternative with spectacular photoelectric properties are suitable for portable integrated photo-rechargeable ESSs, provided they can reach the required level of stability.

3) Further study should be done on solar cells or photoelectrodes working under non-optimal bias voltage conditions during the photo-charging process. Energy level structure and carriers transporting behavior of PC materials could be affected under bias voltage conditions, resulting in decreased photo-charging performance. However, this issue has barely been discussed at present.

4) Regarding solar cell charged ESSs, the investigation on the lifetime of whole device is practically significant. Generally, the lifetime of solar cells is different from that of batteries, thus, once one of them reaches its lifetime, the highly integrated device will face scrapping. Thereby, lifetime matching between solar cells and batteries is a crucial concern.

5) Future efforts for real-world applications should also be paid more attention. The different features of above-mentioned photo-rechargeable ESSs may open their own application directions, such as the use of photocapacitors as a stabilizer for solar cells, the application of photo-batteries in portable electronic device and photo-rechargeable RFBs for the long-term and large-scale solar-driven energy storage power station.

In summary, in the context of the increasingly severe energy problem, we believe that the integrated photo-rechargeable energy storage systems are expected to be the next-generation power source. More efforts will be devoted to this end.

Acknowledgment

The authors acknowledge financial support from the National Natural Science Foundation of China (51720105014).

References

[1] a) S. Chu, Y. Cui, N. Liu, *Nat. Mater.* **2016**, 16, 16; b) L. Zhang, Y. Wang, Z. Niu, J. Chen, *Small Methods* **2019**, 3, 1800443.

[2] A. Gurung, Q. Qiao, *Joule* **2018**, 2, 1217.

[3] M. A. Green, *Nat. Energy* **2016**, 1, 15015.

[4] M. A. Green, *Prog. Photovoltaics* **2001**, 9, 123.

[5] D. Schmidt, M. D. Hager, U. S. Schubert, *Adv. Energy Mater.* **2016**, 6, 1500369.

[6] V. Badescu, *Energy* **2003**, 28, 1165.

[7] N. A. Kelly, T. L. Gibson, *J. Power Sources* **2011**, 196, 10430.

[8] H. Meng, S. Pang, G. Cui, ChemSusChem **2019**, 12, 3431.

[9] J. Bae, Y. J. Park, M. Lee, S. N. Cha, Y. J. Choi, C. S. Lee, J. M. Kim, Z. L. Wang, *Adv. Mater.* **2011**, 23, 3446.

[10] Q. Li, Y. Liu, S. Guo, H. Zhou, *Nano Today* **2017**, 16, 46.

[11] Y. Fu, H. Wu, S. Ye, X. Cai, X. Yu, S. Hou, H. Kafafy, D. Zou, *Energy Environ. Sci.* **2013**, 6, 805.

[12] A. P. Cohn, W. R. Erwin, K. Share, L. Oakes, A. S. Westover, R. E. Carter, R. Bardhan, C. L. Pint, *Nano Lett.* **2015**, 15, 2727.

[13] a) Y. Shao, M. F. El-Kady, J. Sun, Y. Li, Q. Zhang, M. Zhu, H. Wang, B. Dunn, R. B. Kaner, *Chem. Rev.* **2018**, 118, 9233; b) J. Wang, F. Li, F. Zhu, O. G. Schmidt, *Small Methods* **2019**, 3, 1800367.

[14] a) J. Liang, G. Zhu, C. Wang, Y. Wang, H. Zhu, Y. Hu, H. Lv, R. Chen, L. Ma, T. Chen, Z. Jin, J. Liu, *Adv. Energy Mater.* **2017**, 7, 1601208; b) A. Scalia, A. Varzi, A. Lamberti, E. Tresso, S. Jeong, T. Jacob, S. Passerini, *Sustainable Energy Fuels* **2018**, 2, 968.

[15] T. Miyasaka, T. N. Murakami, *Applied Physics Letters* **2004**, 85, 3932.

[16] M. Grätzel, *J. Photochem. Photobiol. C Photochem. Rev.* **2003**, 4, 145.

[17] H.-W. Chen, C.-Y. Hsu, J.-G. Chen, K.-M. Lee, C.-C. Wang, K.-C. Huang, K.-C. Ho, *J. Power Sources* **2010**, 195, 6225.

[18] T. N. Murakami, N. Kawashima, T. Miyasaka, *Chem. Commun.* **2005**, 26, 3346.

[19] R. Narayanan, P. N. Kumar, M. Deepa, A. K. Srivastava, *Electrochim. Acta* **2015**, 178, 113.

[20] Z. Yang, L. Li, Y. Luo, R. He, L. Qiu, H. Lin, H. Peng, *J. Mater. Chem. A* **2013**, 1, 954.

[21] A. Scalia, F. Bella, A. Lamberti, S. Bianco, C. Gerbaldi, E. Tresso, C. F. Pirri, *J. Power Sources* **2017**, 359, 311.

[22] P. Dong, M.-T. F. Rodrigues, J. Zhang, R. S. Borges, K. Kalaga, A. L. M. Reddy, G. G. Silva, P. M. Ajayan, J. Lou, *Nano Energy* **2017**, 42, 181.

[23] Y.-H. Lee, J.-S. Kim, J. Noh, I. Lee, H. J. Kim, S. Choi, J. Seo, S. Jeon, T.-S. Kim, J.-Y. Lee, J. W. Choi, *Nano Lett.* **2013**, 13, 5753.

[24] A. Kumar, D. M. Welsh, M. C. Morvant, F. Piroux, K. A. Abboud, J. R. Reynolds, *Chem. Mater.* **1998**, 10, 896.

[25] C.-Y. Hsu, H.-W. Chen, K.-M. Lee, C.-W. Hu, K.-C. Ho, *J. Power Sources* **2010**, 195, 6232.

[26] A. Das, S. Deshagani, R. Kumar, M. Deepa, *ACS Appl. Mater. Interfaces* **2018**, 10, 35932.

[27] X. Xue, P. Deng, S. Yuan, Y. Nie, B. He, L. Xing, Y. Zhang, *Energy Environ. Sci.* **2013**, 6, 2615.

[28] F. Khatun, P. Thakur, N. Amin Hoque, A. Kool, S. Roy, P. Biswas, B. Bagchi, S. Das, *Energy Convers. Manage.* **2018**, 171, 1083.

[29] C.-W. Lo, C. Li, H. Jiang, *AIP Adv.* **2011**, 1, 042104.

[30] X. Zhang, X. Huang, C. Li, H. Jiang, *Adv. Mater.* **2013**, 25, 4093.

[31] F. Khatun, P. Thakur, A. Kool, S. Roy, N. A. Hoque, P. Biswas, B. Bagchi, S. Das, *Langmuir* **2019**, 35, 6346.

[32] P. Liu, H. X. Yang, X. P. Ai, G. R. Li, X. P. Gao, *Electrochem. Commun.* **2012**, 16, 69.

[33] S. C. Lau, H. N. Lim, T. B. S. A. Ravoof, M. H. Yaacob, D. M. Grant, R. C. I. MacKenzie, I. Harrison, N. M. Huang, *Electrochim. Acta* **2017**, 238, 178.

[34] P. A. Mini, S. V. Nair, K. R. V. Subramanian, *Prog. Photovoltaics* **2013**, 21, 1153.

[35] J. Xu, H. Wu, L. Lu, S.-F. Leung, D. Chen, X. Chen, Z. Fan, G. Shen, D. Li, *Adv. Funct. Mater.* **2014**, 24, 1840.

[36] F. Zhang, W. Li, Z. Xu, M. Ye, W. Guo, H. Xu, X. Liu, *RSC Adv.* **2017**, 7, 52988.

[37] M. Skunik-Nuckowska, K. Grzejszczyk, P. J. Kulesza, L. Yang, N. Vlachopoulos, L. Häggman, E. Johansson, A. Hagfeldt, *J. Power Sources* **2013**, 234, 91.

[38] N. Bagheri, A. Aghaei, M. Y. Ghotbi, E. Marzbanrad, N. Vlachopoulos, L. Häggman, M. Wang, G. Boschloo, A. Hagfeldt, M. Skunik-Nuckowska, P. J. Kulesza, *Electrochim. Acta* **2014**, 143, 390.

[39] a) Q. Xu, D. Yang, J. Lv, Y.-Y. Sun, L. Zhang, *Small Methods* **2018**, 2, 1700316; b) Y. Di, Q. Zeng, C. Huang, D. Tang, K. Sun, C. Yan, Y. Wang, S. Ke, L. Jiang, X. Hao, Y. Lai, F. Liu, *Sol. Energy Mater. Sol. Cells* **2018**, 185, 130.

[40] C. Eames, J. M. Frost, P. R. F. Barnes, B. C. O'Regan, A. Walsh, M. S. Islam, *Nat. Commun.* **2015**, 6, 7497.

[41] Q. Zeng, Y. Di, C. Huang, K. Sun, Y. Zhao, H. Xie, D. Niu, L. Jiang, X. Hao, Y. Lai, F. Liu, *J. Mater. Chem. C* **2018**, 6, 7989.

[42] J. Liang, G. Zhu, Z. Lu, P. Zhao, C. Wang, Y. Ma, Z. Xu, Y. Wang, Y. Hu, L. Ma, T. Chen, Z. Tie, J. Liu, Z. Jin, *J. Mater. Chem. A* **2018**, 6, 2047.

[43] a) B. Farhadi, J. Marriam, S. Yang, H. Zhang, M. Tebyetekerwa, M. Zhu, S. Ramakrishna, R. Jose, F. Zabihi, *J. Power Sources* **2019**, 422, 196; b) C. Li, S. Cong, Z. Tian, Y. Song, L. Yu, C. Lu, Y. Shao, J. Li, G. Zou, M. H. Rümmeli, S. Dou, J. Sun, Z. Liu, *Nano Energy* **2019**, 60, 247; c) X. Xu, S. Li, H. Zhang, Y. Shen, S. M. Zakeeruddin, M. Graetzel, Y.-B. Cheng, M. Wang, *ACS Nano* **2015**, 9, 1782.

[44] a) Z. Wu, P. Li, Y. Zhang, Z. Zheng, *Small Methods* **2018**, 2, 1800031; b) L. Cai, G. Yu, *Small Methods* **2019**, 3, 1900071.

[45] J. Xu, Z. Ku, Y. Zhang, D. Chao, H. J. Fan, *Adv. Mater. Technol.* **2016**, 1, 1600074.

[46] J. You, L. Meng, T.-B. Song, T.-F. Guo, Y. Yang, W.-H. Chang, Z. Hong, H. Chen, H. Zhou, Q. Chen, Y. Liu, N. De Marco, Y. Yang, *Nat. Nanotech.* **2015**, 11, 75.

[47] R. Liu, C. Liu, S. Fan, *J. Mater. Chem. A* **2017**, 5, 23078.

[48] C. H. Ng, H. N. Lim, S. Hayase, Z. Zainal, S. Shafie, H. W. Lee, N. M. Huang, *ACS Appl. Energy Mater.* **2018**, 1, 692.

[49] J. Liang, G. Zhu, C. Wang, P. Zhao, Y. Wang, Y. Hu, L. Ma, Z. Tie, J. Liu, Z. Jin, *Nano Energy* **2018**, 52, 239.

[50] G. Wee, T. Salim, Y. M. Lam, S. G. Mhaisalkar, M. Srinivasan, *Energy Environ. Sci.* **2011**, 4, 413.

[51] L. Meng, Y. Zhang, X. Wan, C. Li, X. Zhang, Y. Wang, X. Ke, Z. Xiao, L. Ding, R. Xia, H.-L. Yip, Y. Cao, Y. Chen, *Science* **2018**, 361, 1094.

[52] Z. Zhang, X. Chen, P. Chen, G. Guan, L. Qiu, H. Lin, Z. Yang, W. Bai, Y. Luo, H. Peng, *Adv. Mater.* **2014**, 26, 466.

[53] C.-T. Chien, P. Hiralal, D.-Y. Wang, I. S. Huang, C.-C. Chen, C.-W. Chen, G. A. J. Amaratunga, *Small* **2015**, 11, 2929.

[54] Y. Jin, Z. Li, L. Qin, X. Liu, L. Mao, Y. Wang, F. Qin, Y. Liu, Y. Zhou, F. Zhang, *Adv. Mater. Interfaces* **2017**, 4, 1700704.

[55] B. P. Lechêne, M. Cowell, A. Pierre, J. W. Evans, P. K. Wright, A. C. Arias, *Nano Energy* **2016**, 26, 631.

[56] J. Kim, S. M. Lee, Y.-H. Hwang, S. Lee, B. Park, J.-H. Jang, K. Lee, *J. Mater. Chem. A* **2017**, 5, 1906.

[57] J. Yuan, Y. Zhang, L. Zhou, G. Zhang, H.-L. Yip, T.-K. Lau, X. Lu, C. Zhu, H. Peng, P. A. Johnson, M. Leclerc, Y. Cao, J. Ulanski, Y. Li, Y. Zou, *Joule* **2019**, 3, 1140.

[58] T. Tatsuma, S. Saitoh, Y. Ohko, A. Fujishima, *Chem. Mater.* **2001**, 13, 2838.

[59] A. Takshi, H. Yaghoubi, T. Tevi, S. Bakhshi, *J. Power Sources* **2015**, 275, 621.

[60] J. Cai, C. Lv, A. Watanabe, *RSC Adv.* **2017**, 7, 415.

[61] Y. Huang, Y. Zeng, M. Yu, P. Liu, Y. Tong, F. Cheng, X. Lu, *Small Methods* **2018**, 2, 1700230.

[62] S. Safshekan, I. Herraiz-Cardona, D. Cardenas-Morcoso, R. Ojani, M. Haro, S. Gimenez, *ACS Energy Lett.* **2017**, 2, 469.

[63] X. Xia, J. Luo, Z. Zeng, C. Guan, Y. Zhang, J. Tu, H. Zhang, H. J. Fan, *Sci. Rep.* **2012**, 2, 981.

[64] Y. Wang, J. Tang, Z. Peng, Y. Wang, D. Jia, B. Kong, A. A. Elzatahry, D. Zhao, G. Zheng, *Nano Lett.* **2014**, 14, 3668.

[65] K. Maeda, K. Domen, *J. Phys. Chem. Lett.* **2010**, 1, 2655.

[66] K. Zhu, G. Zhu, J. Wang, J. Zhu, G. Sun, Y. Zhang, P. Li, Y. Zhu, W. Luo, Z. Zou, W. Huang, *J. Mater. Chem. A* **2018**, 6, 21360.

[67] J. Wang, Y. Pan, L. Jiang, M. Liu, F. Liu, M. Jia, J. Li, Y. Lai, *ACS Appl. Mater. Interfaces* **2019**, 11, 37541.

[68] M. Zhu, Y. Huang, Y. Huang, Z. Pei, Q. Xue, H. Li, H. Geng, C. Zhi, *Adv. Funct. Mater.* **2016**, 26, 4481.

[69] a) S. Kalasina, P. Pattanasattayavong, M. Suksomboon, N. Phattharasupakun, J. Wutthiprom, M. Sawangphruk, *Chem. Commun.* **2017**, 53, 709; b) S. Kalasina, N. Phattharasupakun, T. Maihom, V. Promarak, T. Sudyoadsuk, J. Limtrakul, M. Sawangphruk, *Sci. Rep.* **2018**, 8, 12192.

[70] S. Kalasina, K. Kongsawatvoragul, N. Phattharasupakun, M. Sawangphruk, *J. Electrochem. Soc.* **2019**, 166, A2444.

[71] Y. Cui, Y.-X. Pan, H. Qin, H.-P. Cong, S.-H. Yu, *Small Methods* **2018**, 2, 1800029.

[72] C. An, Z. Wang, W. Xi, K. Wang, X. Liu, Y. Ding, *J. Mater. Chem. A* **2019**, 7, 15691.

[73] H. Liu, M. Li, R. B. Kaner, S. Chen, Q. Pei, *ACS Appl. Mater. Interfaces* **2018**, 10, 15609.

[74] a) B. Dunn, H. Kamath, J.-M. Tarascon, *Science* **2011**, 334, 928; b) J. A. Lochala, H. Zhang, Y. Wang, O. Okolo, X. Li, J. Xiao, *Small Methods* **2017**, 1, 1700099.

[75] J. B. Goodenough, K.-S. Park, *J. Am. Chem. Soc.* **2013**, 135, 1167.

[76] S. S. Zhang, *J. Power Sources* **2006**, 161, 1385.

[77] K. Ithisuphalap, H. Zhang, L. Guo, Q. Yang, H. Yang, G. Wu, *Small Methods* **2019**, 3, 1800352.

[78] B. Luo, D. Ye, L. Wang, *Adv. Sci.* **2017**, 4, 1700104.

[79] Q. Li, N. Li, M. Ishida, H. Zhou, *J. Mater. Chem. A* **2015**, 3, 20903.

[80] X. Liu, Y. Yuan, J. Liu, B. Liu, X. Chen, J. Ding, X. Han, Y. Deng, C. Zhong, W. Hu, *Nat. Commun.* **2019**, 10, 4767.

[81] A. Lee, M. Vörös, W. M. Dose, J. Niklas, O. Poluektov, R. D. Schaller, H. Iddir, V. A. Maroni, E. Lee, B. Ingram, L. A. Curtiss, C. S. Johnson, *Nat. Commun.* **2019**, 10, 4946.

[82] M. Grätzel, *Nature* **2001**, 414, 338.

[83] L.-X. Yuan, Z.-H. Wang, W.-X. Zhang, X.-L. Hu, J.-T. Chen, Y.-H. Huang, J. B. Goodenough, *Energy Environ. Sci.* **2011**, 4, 269.

[84] W. Guo, X. Xue, S. Wang, C. Lin, Z. L. Wang, *Nano Lett.* **2012**, 12, 2520.

[85] S. N. Agbo, T. Merdzhanova, S. Yu, H. Tempel, H. Kungl, R.-A. Eichel, U. Rau, O. Astakhov, *J. Power Sources* **2016**, 327, 340.

[86] H.-D. Um, K.-H. Choi, I. Hwang, S.-H. Kim, K. Seo, S.-Y. Lee, *Energy Environ. Sci.* **2017**, 10, 931.

[87] J. Xu, Y. Chen, L. Dai, *Nat. Commun.* **2015**, 6, 8103.

[88] G.-M. Weng, J. Kong, H. Wang, C. Karpovich, J. Lipton, F. Antonio, Z. S. Fishman, H. Wang, W. Yuan, A. D. Taylor, *Energy Storage Mater.* **2020,** 24, **557**

[89] A. Paolella, C. Faure, G. Bertoni, S. Marras, A. Guerfi, A. Darwiche, P. Hovington, B. Commarieu, Z. Wang, M. Prato, M. Colombo, S. Monaco, W. Zhu, Z. Feng, A. Vijh, C. George, G. P. Demopoulos, M. Armand, K. Zaghib, *Nat. Commun.* **2017**, 8, 14643.

[90] J.-H. Jeong, D.-w. Jung, E. W. Shin, E.-S. Oh, *J. Alloys Compd.* **2014**, 604, 226

[91] J. Jin, L. Wu, S. Huang, M. Yan, H. Wang, L. Chen, T. Hasan, Y. Li, B.-L. Su, *Small Methods* **2018**, 2, 1800171.

[92] O. Nguyen, E. Courtin, F. Sauvage, N. Krins, C. Sanchez, C. Laberty-Robert, *J. Mater. Chem. A* **2017**, 5, 5927.

[93] C. Andriamiadamanana, I. Sagaidak, G. Bouteau, C. Davoisne, C. Laberty-Robert, F. Sauvage, *Adv. Sust. Syst.* **2018**, 2, 1700166.

[94] H.-R. Xia, W.-T. Sun, L.-M. Peng, *Chem. Commun.* **2015**, 51, 13787.

[95] S. Ahmad, C. George, D. J. Beesley, J. J. Baumberg, M. De Volder, *Nano Lett.* **2018**, 18, 1856.

[96] C. Zhao, Y. Lu, Y. Li, L. Jiang, X. Rong, Y.-S. Hu, H. Li, L. Chen, *Small Methods* **2017**, 1, 1600063.

[97] a) Y.-Y. Gui, F.-X. Ai, J.-F. Qian, Y.-L. Cao, G.-R. Li, X.-P. Gao, H.-X. Yang, *J. Mater. Chem. A* **2018**, 6, 10627; b) B. Senthilkumar, C. Murugesan, L. Sharma, S. Lochab, P. Barpanda, *Small Methods* **2019**, 3, 1800253.

[98] Q. Li, N. Li, Y. Liu, Y. Wang, H. Zhou, *Adv. Energy Mater.* **2016**, 6, 1600632.

[99] Z. Tian, C. Li, J. Cai, L. Zhang, C. Lu, Y. Song, T. Jiang, J. Sun, S. Dou, *Chem. Commun.* **2019**, 55, 1291.

[100] a) Y. Gao, C. Zhu, Z. Chen, G. Lu, *J. Phys. Chem. C* **2017**, 121, 7131; b) S. C. Jung, Y.-J. Kang, D.-J. Yoo, J. W. Choi, Y.-K. Han, *J. Phys. Chem. C* **2016**, 120, 13384; c) M.-C. Lin, M. Gong, B. Lu, Y. Wu, D.-Y. Wang, M. Guan, M. Angell, C. Chen, J. Yang, B.-J. Hwang, H. Dai, *Nature* **2015**, 520, 324.

[101] Y. Hu, Y. Bai, B. Luo, S. Wang, H. Hu, P. Chen, M. Lyu, J. Shapter, A. Rowan, L. Wang, *Adv. Energy Mater.* **2019**, 9, 1900872.

[102] W. Dai, X. Cui, Y. Zhou, Y. Zhao, L. Wang, L. Peng, W. Chen, *Small Methods* **2019**, 3, 1800358.

[103] B. D. McCloskey, A. Speidel, R. Scheffler, D. C. Miller, V. Viswanathan, J. S. Hummelshøj, J. K. Nørskov, A. C. Luntz, *J. Phys. Chem. Lett.* **2012**, 3, 997.

[104] a) Y. Chen, S. A. Freunberger, Z. Peng, O. Fontaine, P. G. Bruce, Nature Chemistry **2013**, 5, 489; b) H.-D. Lim, H. Song, J. Kim, H. Gwon, Y. Bae, K.-Y. Park, J. Hong, H. Kim, T. Kim, Y. H. Kim, X. Lepró, R. Ovalle-Robles, R. H. Baughman, K. Kang, *Angew. Chem. Int. Ed.* **2014**, 53, 3926.

[105] M. Yu, X. Ren, L. Ma, Y. Wu, *Nat. Commun.* **2014**, 5, 5111.

[106] Y. Liu, N. Li, S. Wu, K. Liao, K. Zhu, J. Yi, H. Zhou, *Energy Environ. Sci.* **2015**, 8, 2664.

[107] Y. Liu, N. Li, K. Liao, Q. Li, M. Ishida, H. Zhou, *J. Mater. Chem. A* **2016**, 4, 12411.

[108] Y. Qiao, Y. Liu, K. Jiang, X. Li, Y. He, Q. Li, S. Wu, H. Zhou, *Small Methods* **2018**, 2, 1700284.

[109] Y. Li, M. Gong, Y. Liang, J. Feng, J.-E. Kim, H. Wang, G. Hong, B. Zhang, H. Dai, *Nat. Commun.* **2013**, 4, 1805.

[110] a) D. Yang, L. Zhang, X. Yan, X. Yao, *Small Methods* **2017**, 1, 1700209; b) Z. Fang, Y. Zhang, X. Hu, X. Fu, L. Dai, D. Yu, *Angew. Chem. Int. Ed.* **2019**, 58, 9248.

[111] D. Zhu, Q. Zhao, G. Fan, S. Zhao, L. Wang, F. Li, J. Chen, *Angew. Chem. Int. Ed.* **2019**, 58, 12460.

[112] Y. Jiang, Q. Wang, L. Han, X. Zhang, L. Jiang, Z. Wu, Y. Lai, D. Wang, F. Liu, *Chem. Eng. J.* **2019**, 358, 752.

[113] Y. Zhao, N. B. Mercier, H. R. Byon, *ChemPlusChem* **2015**, 80, 344.

[114] M. Yu, W. D. McCulloch, D. R. Beauchamp, Z. Huang, X. Ren, Y. Wu, *J. Am. Chem. Soc.* **2015**, 137, 8332.

[115] W. Zhao, X.-F. Wang, E. Zheng, Y. Wei, Y. Sanehira, G. Chen, *J. Power Sources* **2017**, 350, 28.

[116] a) J. Jasieniak, M. Califano, S. E. Watkins, *ACS Nano* **2011**, 5, 5888; b) A. G. Tamirat, J. Rick, A. A. Dubale, W.-N. Su, B.-J. Hwang, *Nanoscale Horiz.* **2016**, 1, 243.

[117] Z. Wang, H.-C. Chiu, A. Paolella, K. Zaghib, G. P. Demopoulos, *ChemSusChem* **2019**, 12, 2220.

[118] B. Lei, G.-R. Li, P. Chen, X.-P. Gao, *ACS Appl. Energy Mater.* **2019**, 2, 1000.

[119] a) Y. Lin, G. Yuan, S. Sheehan, S. Zhou, D. Wang, *Energy Environ. Sci.* **2011**, 4, 4862; b) B. Klahr, S. Gimenez, F. Fabregat-Santiago, T. Hamann, J. Bisquert, *J. Am. Chem. Soc.* **2012**, 134, 4294; c) S. Tanaka, Y. V. Kaneti, N. L. W. Septiani, S. X. Dou, Y. Bando, M. S. A. Hossain, J. Kim, Y. Yamauchi, *Small Methods* **2019**, 3, 1800512.

[120] G. Nikiforidis, K. Tajima, H. R. Byon, *ACS Energy Lett.* **2016**, 1, 806.

[121] G. Zhang, Z.-W. Zhang, H.-J. Peng, J.-Q. Huang, Q. Zhang, *Small Methods* **2017**, 1, 1700134.

[122] a) Z. Deng, Z. Zhang, Y. Lai, J. Liu, J. Li, Y. Liu, *J. Electrochem. Soc.* **2013**, 160, A553; b) M. Li, Z. Amirzadeh, R. De Marco, X. F. Tan, A. Whittaker, X. Huang, R. Wepf, R. Knibbe, *Small Methods* **2018**, 2, 1800133.

[123] P. Chen, G.-R. Li, T.-T. Li, X.-P. Gao, *Adv. Sci.* **2019**, 6, 1900620.

[124] A. Yermukhambetova, C. Tan, S. R. Daemi, Z. Bakenov, J. A. Darr, D. J. L. Brett, P. R. Shearing, *Sci. Rep.* **2016**, 6, 35291.

[125] X. Zang, L. Yan, Y. Yang, H. Pan, Z. Nie, K. W. Jung, Z. D. Deng, W. Wang, *Small Methods* **2019**, 0, 1900494.

[126] W. Wang, Q. Luo, B. Li, X. Wei, L. Li, Z. Yang, *Adv. Funct. Mater.* **2013**, 23, 970.

[127] Z. Wei, D. Liu, C. Hsu, F. Liu, *Electrochem. Commun.* **2014**, 45, 79.

[128] J. Azevedo, T. Seipp, J. Burfeind, C. Sousa, A. Bentien, J. P. Araújo, A. Mendes, *Nano Energy* **2016**, 22, 396.

[129] a) D. Liu, W. Zi, S. D. Sajjad, C. Hsu, Y. Shen, M. Wei, F. Liu, *ACS Catal.* **2015**, 5, 2632; b) B. K. Durant, Y. She, P. Wang, T. Kraus, B. A. Parkinson, *J. Electrochem. Soc.* **2019**, 166, H3001.

[130] K. Wedege, J. Azevedo, A. Khataee, A. Bentien, A. Mendes, *Angew. Chem. Int. Ed.* **2016**, 55, 7142.

[131] A. Khataee, J. Azevedo, P. Dias, D. Ivanou, E. Dražević, A. Bentien, A. Mendes, *Nano Energy* **2019**, 62, 832.

[132] W. Li, H.-C. Fu, Y. Zhao, J.-H. He, S. Jin, *Chem* **2018**, 4, 2644.

[133] S. Zhang, C. Chen, Y. Zhou, Y. Qian, J. Ye, S. Xiong, Y. Zhao, X. Zhang, *ACS Appl. Mater. Interfaces* **2018**, 10, 23048.

[134] Y. Zhou, S. Zhang, Y. Ding, L. Zhang, C. Zhang, X. Zhang, Y. Zhao, G. Yu, *Adv. Mater.* **2018**, 30, 1802294.

[135] Y. Zhou, L. Zhang, L. Lin, B. R. Wygant, Y. Liu, Y. Zhu, Y. Zheng, C. B. Mullins, Y. Zhao, X. Zhang, G. Yu, *Nano Lett.* **2017**, 17, 8012.

[136] P. Liu, Y.-l. Cao, G.-R. Li, X.-P. Gao, X.-P. Ai, H.-X. Yang, *ChemSusChem* **2013**, 6, 802.

[137] a) N. F. Yan, G. R. Li, X. P. Gao, *J. Mater. Chem. A* **2013**, 1, 7012; b) N. F. Yan, G. R. Li, X. P. Gao, *J. Electrochem. Soc.* **2014**, 161, A736.

[138] S. Liao, X. Zong, B. Seger, T. Pedersen, T. Yao, C. Ding, J. Shi, J. Chen, C. Li, *Nat. Commun.* **2016**, 7, 11474.

[139] W. Li, H.-C. Fu, L. Li, M. Cabán-Acevedo, J.-H. He, S. Jin, *Angew. Chem. Int. Ed.* **2016**, 55, 13104.

[140] a) L. Hoober-Burkhardt, S. Krishnamoorthy, B. Yang, A. Murali, A. Nirmalchandar, G. K. S. Prakash, S. R. Narayanan, *J. Electrochem. Soc.* **2017**, 164, A600; b) M. G. Walter, E. L. Warren, J. R. McKone, S. W. Boettcher, Q. Mi, E. A. Santori, N. S. Lewis, *Chem. Rev.* **2010**, 110, 6446.

[141] W. Li, E. Kerr, M.-A. Goulet, H.-C. Fu, Y. Zhao, Y. Yang, A. Veyssal, J.-H. He, R. G. Gordon, M. J. Aziz, S. Jin, *Adv. Energy Mater.* **2019**, 9, 1900918.

[142] Q. Cheng, W. Fan, Y. He, P. Ma, S. Vanka, S. Fan, Z. Mi, D. Wang, *Adv. Mater.* **2017**, 29, 1700312.

[143] T. Chen, L. Qiu, Z. Yang, Z. Cai, J. Ren, H. Li, H. Lin, X. Sun, H. Peng, *Angew. Chem. Int. Ed.* **2012**, 51, 11977.

[144] X. Chen, H. Sun, Z. Yang, G. Guan, Z. Zhang, L. Qiu, H. Peng, *J. Mater. Chem. A* **2014**, 2, 1897.

[145] H. Sun, Y. Jiang, S. Xie, Y. Zhang, J. Ren, A. Ali, S.-G. Doo, I. H. Son, X. Huang, H. Peng, *J. Mater. Chem. A* **2016**, 4, 7601.

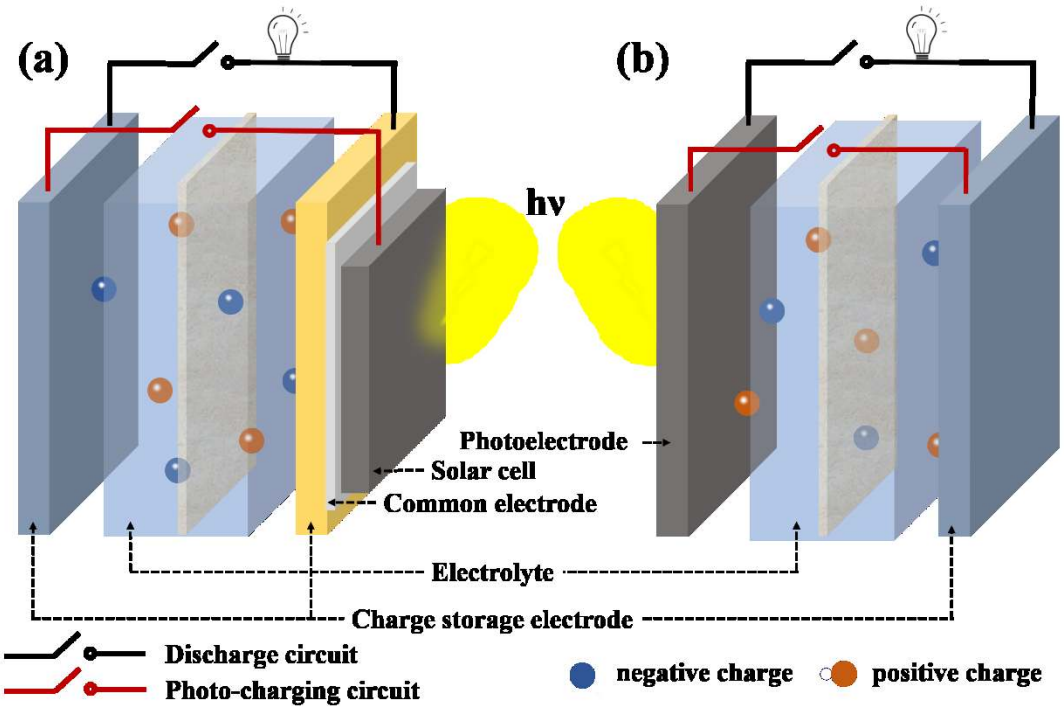

Figure 1. a) Integration of an individual solar cell and ESS. b) Incorporating a dual-functional photoelectrode into ESS.

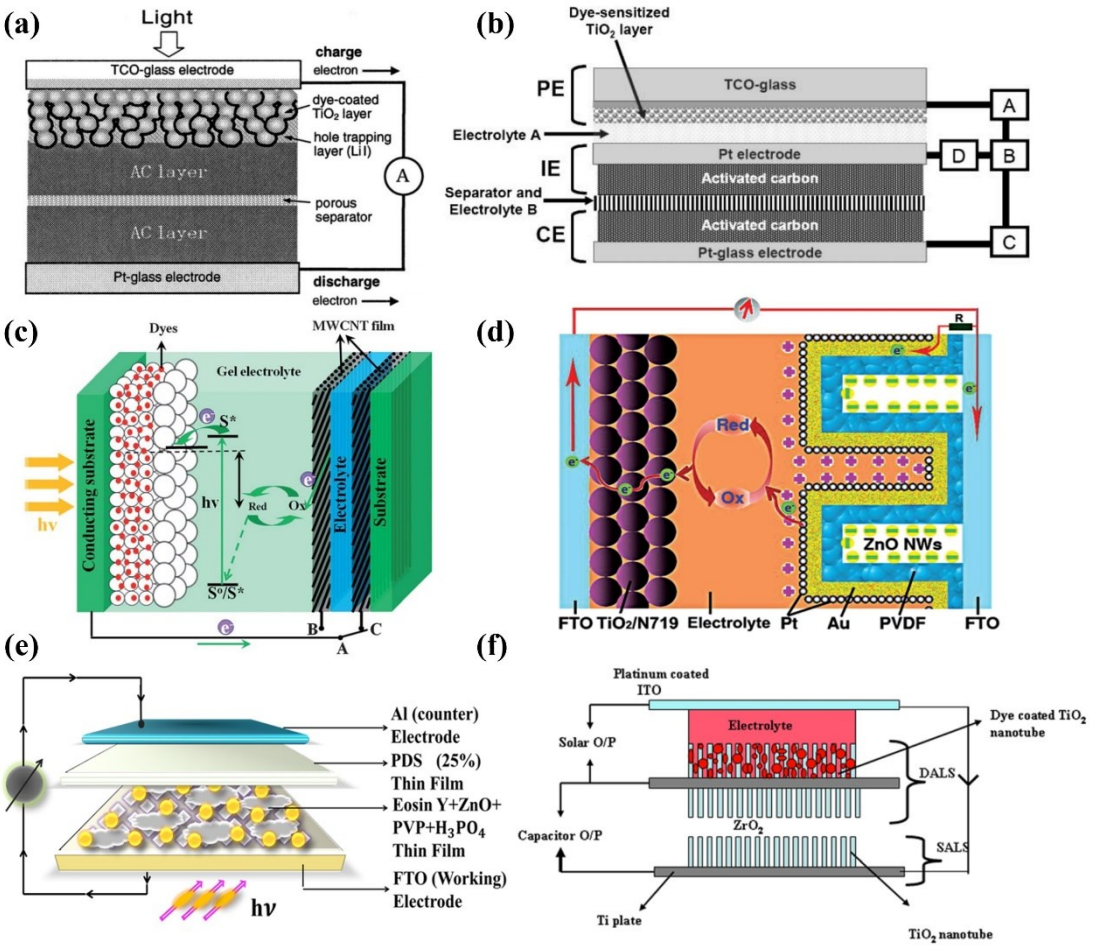

Figure 2. a) Schematic illustration for the two-electrode, sandwich-type multilayered photocapacitor.[15] Copyright 2004, American Institute of Physics. b) Structure of the three-electrode photocapacitor.[18] Copyright 2005, The Royal Society of Chemistry. c) Schematic illustration of an integrated device for both photoelectric conversion and energy storage based on aligned MWCNT films as electrodes.[20] Copyright 2013, Royal Society of Chemistry. d) Schematics of the mechanism of TiO_2 dye-sensitized solar cells with energy storage function by modifying the counter electrode with PVDF/ZNWA nanocomposites.[30] Copyright 2013, WILEY-VCH. e) Symbolic representation of the fabricated PVDF/SDS film in photocapacitor.[31] Copyright 2019, American Chemical Society. f)

Schematic illustration of integrated solar cell with double-anodized titanium plate.[34] Copyright 2012, WILEY-VCH.

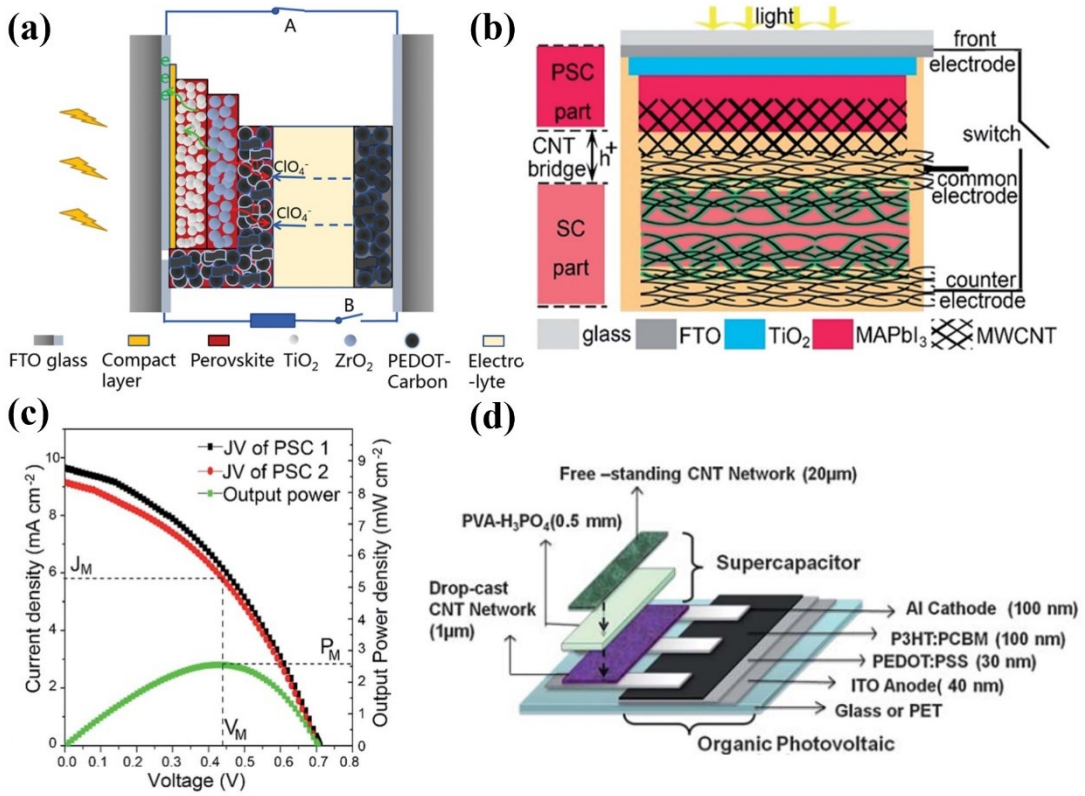

Figure 3. a) Schematic illustration and working mechanism of a perovskite photocapacitor device constructed based on the ClO_4^--doped PEDOT electrode.[45] Copyright 2016, WILEY-VCH. b) Schematic of the photocapacitor based on CNT bridge. c) *J-V* curves of the PSC part before (PSC 1) and after integration (PSC 2), and power output of PSC 2.[47] Copyright 2017, The Royal Society of Chemistry. d) A schematic representation of an OSC-photocapacitor fabricated using the layer-by-layer approach, with the thickness indicated for each layer of components.[50] Copyright 2011, The Royal Society of Chemistry.

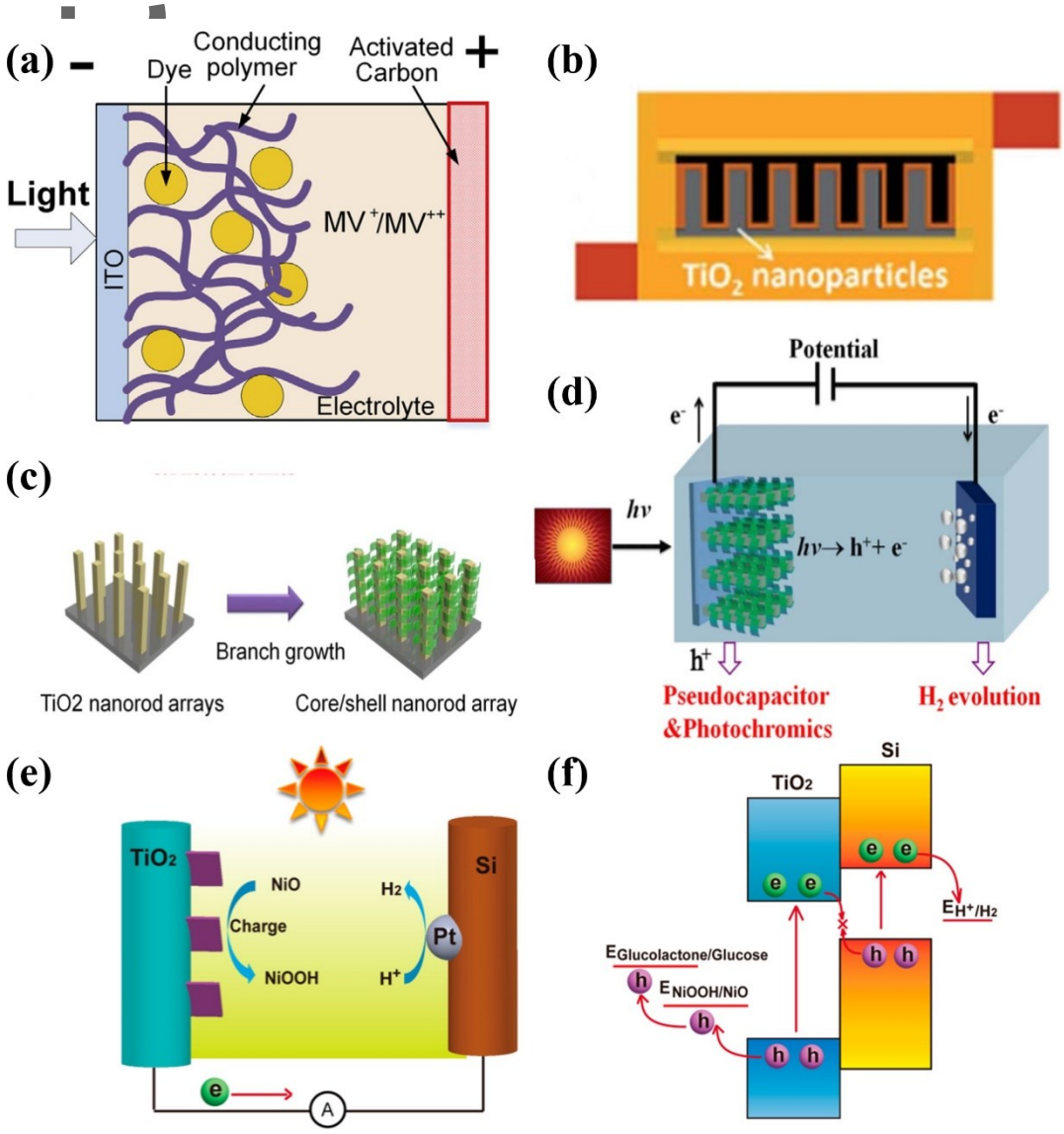

Figure 4. a) Schematic of an electrochemical device with a composite of a conducting polymer and a dye as the photosensitive anode electrode.[59] Copyright 2014, Elsevier B.V. b) Schematic illustration for the fabrication of a carbon/TiO_2 micro-supercapacitor with photo-rechargeable capability.[60] Copyright 2017, The Royal Society of Chemistry. c) Synthesis of the core/shell nanorod arrays by a two-step solution method: hydrothermal for TiO_2 core, followed by chemical bath deposition or

electrodeposition for the branch. d) Concept of the device based on TiO_2 and transition metal oxides/hydroxides core/shell nanorod arrays.[63] Copyright 2012, Nature Publishing Group. e) Solar-powered mechanism of the TiO_2/NiO photoanode and the Si/Pt photocathode for the solar-powered pseudocapacitive system. f) Energy diagram of the system.[64] Copyright 2014, American Chemical Society.

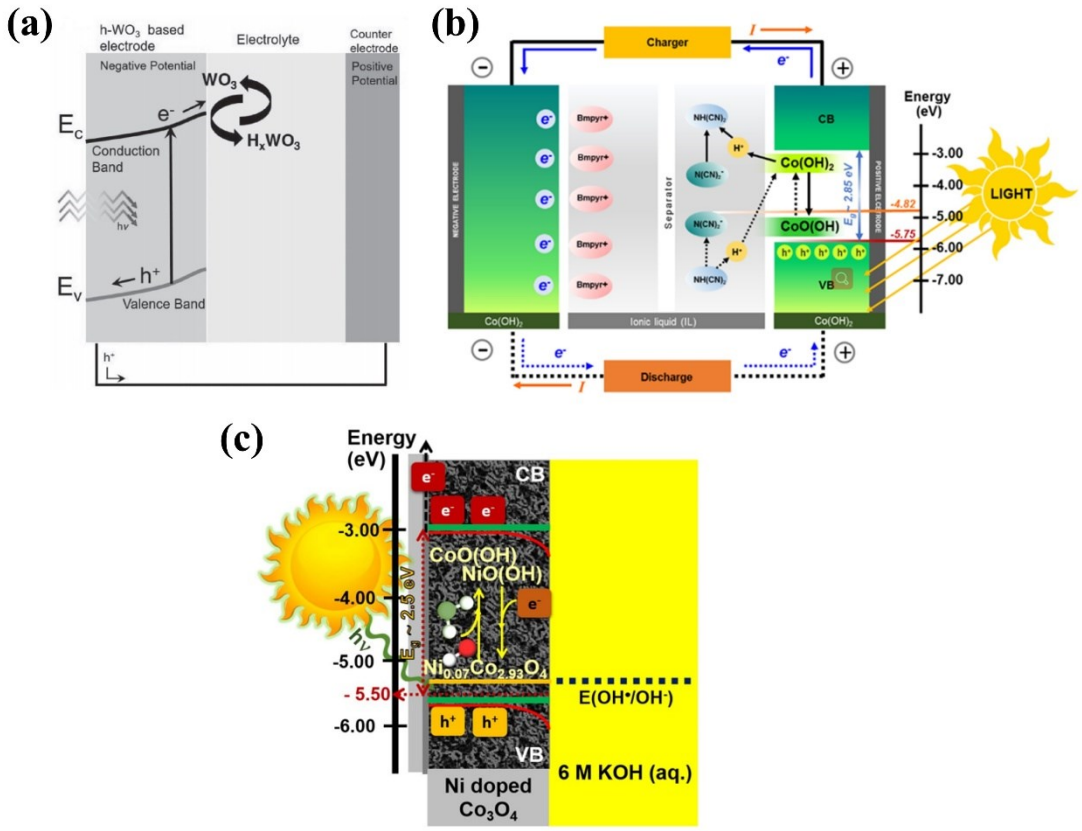

Figure 5. a) The schematic mechanism of the increments of capacitance under illumination of solar light.[68] Copyright 2016, WILEY-VCH. b) The schematic of the charge storage mechanism of the symmetric $Co(OH)_2$ photocapacitors under light illumination.[69b] Copyright 2018, Nature Publishing Group. c) The energy diagram of $Ni_{0.07}Co_{2.93}O_4$ nanosheets in KOH

Electrolyte.[70] Copyright 2019, The Electrochemical Society.

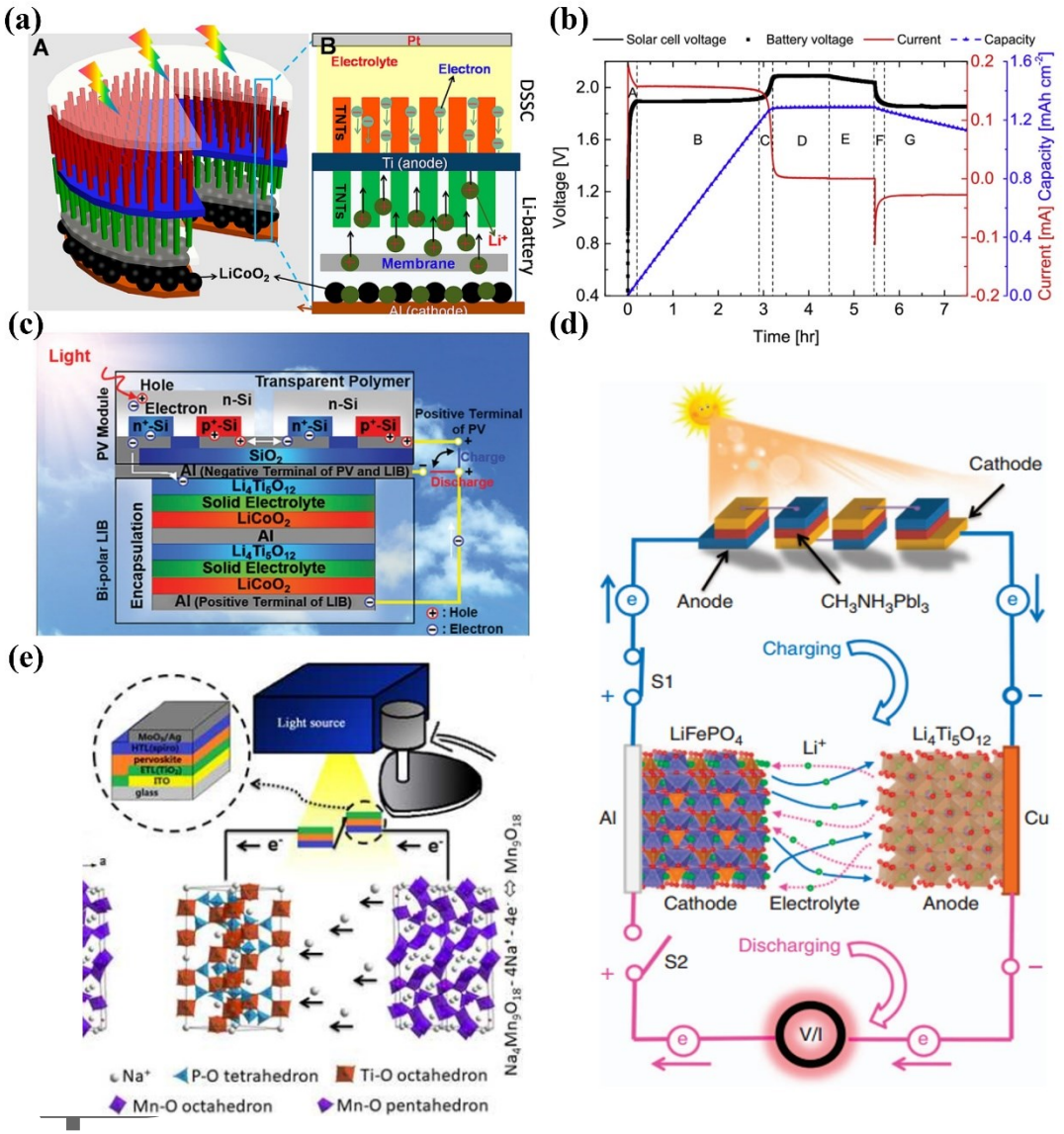

Figure 6. a) Schematic of an integrated DSSC-charged LIB based on double-sided TiO_2 nanotube arrays. Among, A: TiO_2 nanotube arrays grown on the Ti foil substrate by anodization in fluoric

ethylene glycol solution. B: Detailed structure and working principle of the DSSC-charged LIB.[84] Copyright 2012, American Chemical Society. b) Charge/discharge test cycle of the LIB connected to the triple junction solar cell. Voltage of the solar cell, charging current, voltage and capacity of the storage cell are presented on the time scale.[85] Copyright 2016, Elsevier B.V. c) Schematic representation of the internal structure and operating principle of the Si-LIB device under sunlight illumination.[86] Copyright 2017, The Royal Society of Chemistry. d) Schematic diagram of the fabricated system of PSC-LIB.[87] Copyright 2015, Nature Publishing Group. e) Schematic illustration of the working mechanism of PSC based photo-battery under illumination.[88] Copyright 2019, Elsevier B.V.

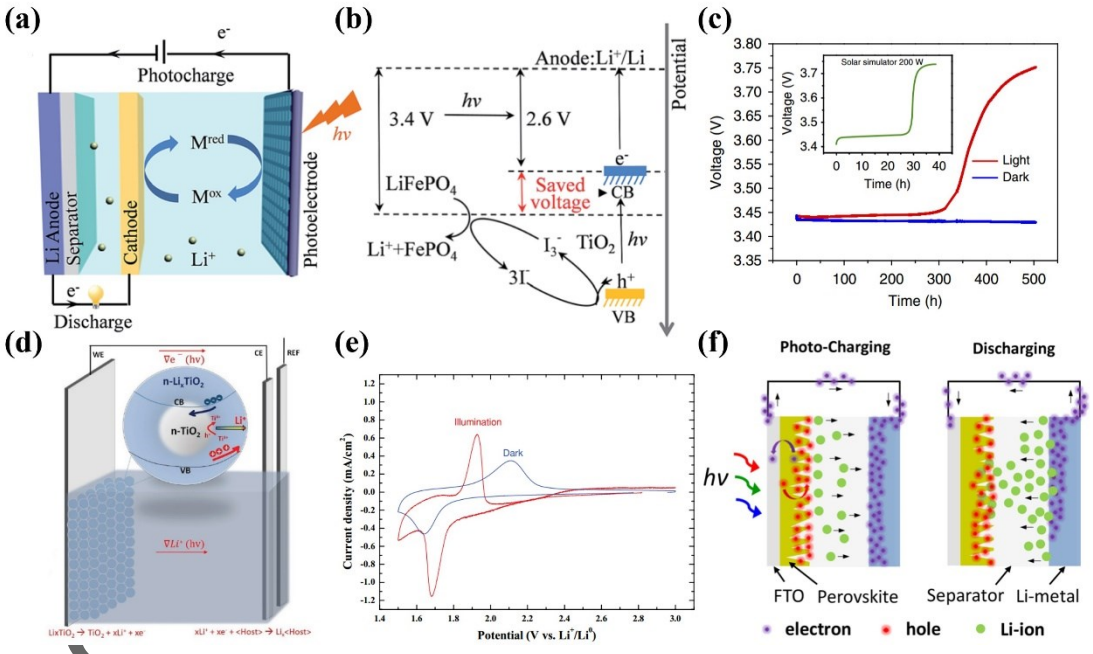

Figure 7. a) Schematic illustration of a photo-rechargeable LIB with a TiO_2 photoelectrode. b) The energy diagram of the photo-rechargeable LIB. The saved voltage is determined by the energy difference between the charging voltage of the LIB and the quasi-Fermi level (E_f) of electrons in the semiconductor (near to its CB).[79] Copyright 2015, The Royal Society of Chemistry. c) The voltage of

LFP/dye electrode after a plateau at 3.40 V increased to 3.75 V under Neon light exposure and in the dark using a black box (blue line), the voltage slightly decreases from 3.44 to 3.41 V in 500 h. The inset shows the change in voltage upon illumination with a solar simulator (green line).[89] Copyright 2017, Nature Publishing Group. d) Bandgap excitation, photo-oxidation, and Li^+ reduction when the device is exposed to incident light. e) Comparison of CV under dark and illumination for Li_xTiO_2 photoelectrode.[93] Copyright 2018, WILEY-VCH. f) Schematics of the charge generation, transfer, and storage mechanisms in perovskite electrode under light illumination.[95] Copyright 2018, American Chemical Society.

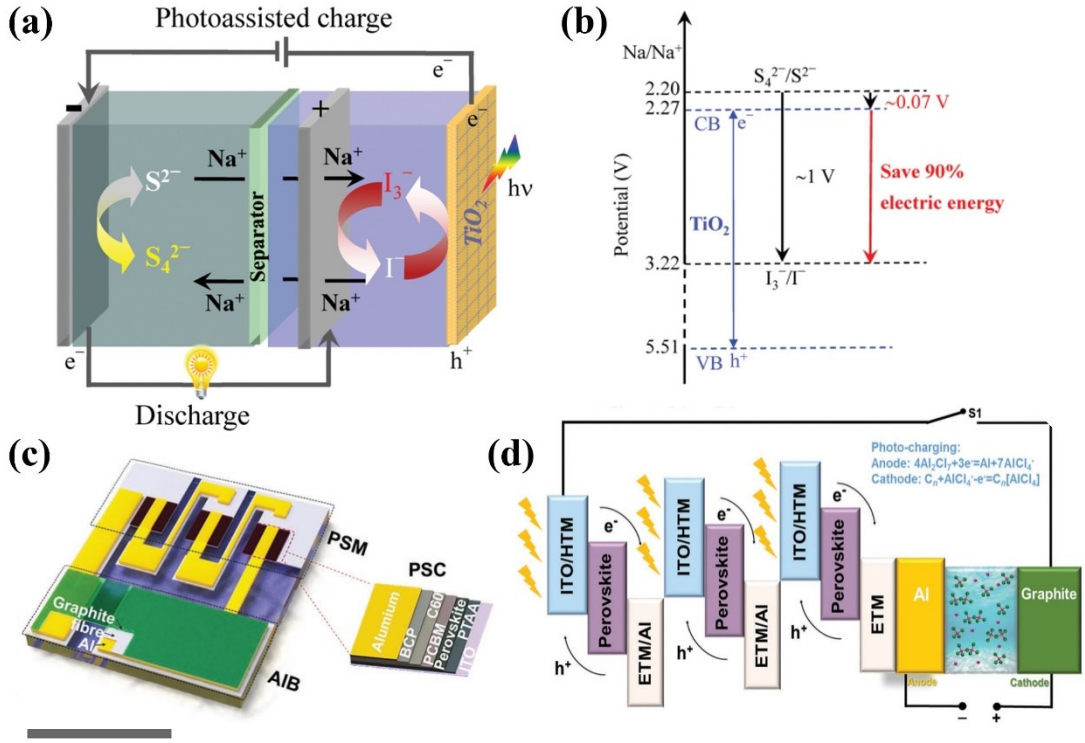

Figure 8. a) Schematic of a photo-assisted rechargeable NIB with a three-electrode system including a TiO_2 photoelectrode. b) Potential diagram for the photo-assisted charging process.[98] Copyright 2016, WILEY-VCH. c) Diagram of the integrated PSM-AIB solar-rechargeable battery and a single

PSC. In the PSC, ITO, PTAA, PCBM, and BCP represent the indium-doped tin oxide, poly(triarylamie), phenyl-C_{61}-butyric acid methyl ester, and bathocuproine layers, respectively. d) Device structure of the PSM-AIB system with the photo-charging mechanism.[101] Copyright 2019, WILEY-VCH.

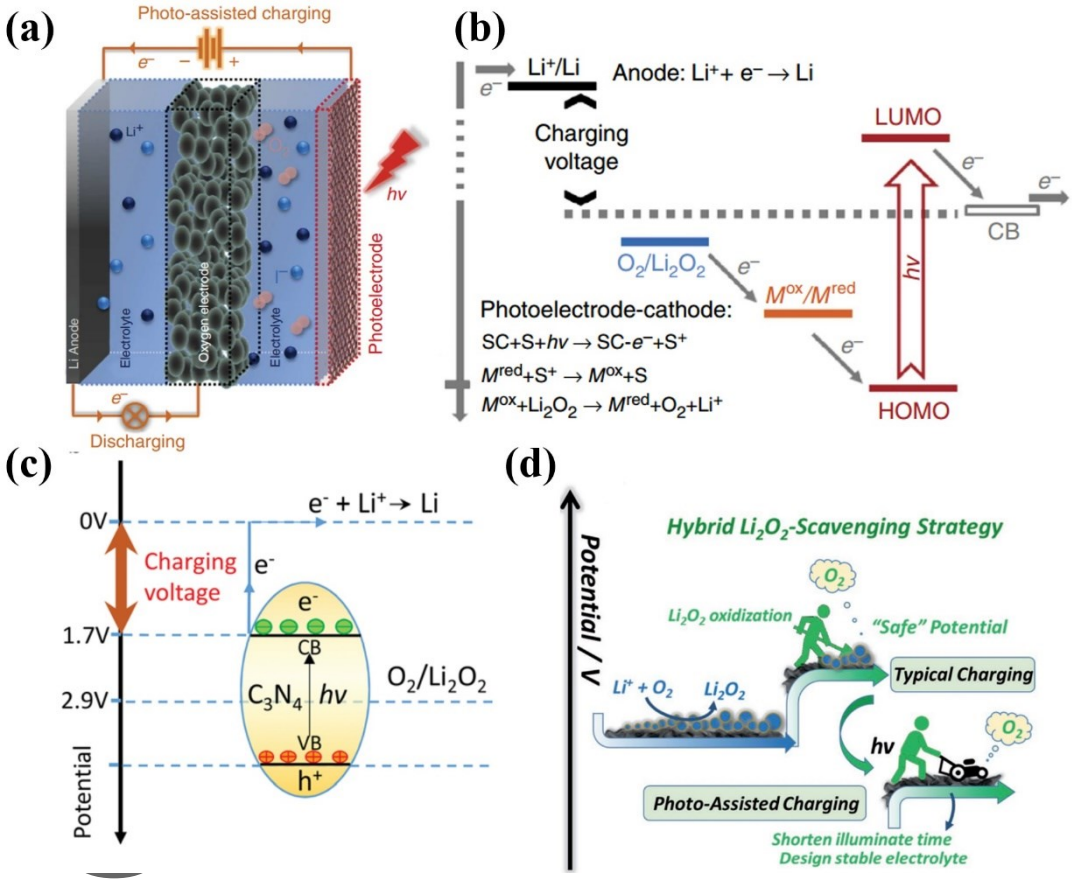

Figure 9. a) The scheme of a three-electrode photo-battery consisting of a Li anode, an oxygen electrode and a photoelectrode. b) Potential diagram for the photo-assisted charging process.[105] Copyright 2016, WILEY-VCH. c) The theoretical potential diagram illustrates the photo-assisted charge voltage equals the energy difference between the redox potential of the Li^+/Li couple and CB of g-C_3N_4 (1.7 V).[107] Copyright 2016, The Royal Society of Chemistry. d) Schematic for the newly

designed hybrid charging strategy, integrated by a typical charging process upon low overpotential stage and a subsequent photo-assisted Li_2O_2-scavenged charging process.[108] Copyright 2017, WILEY-VCH.

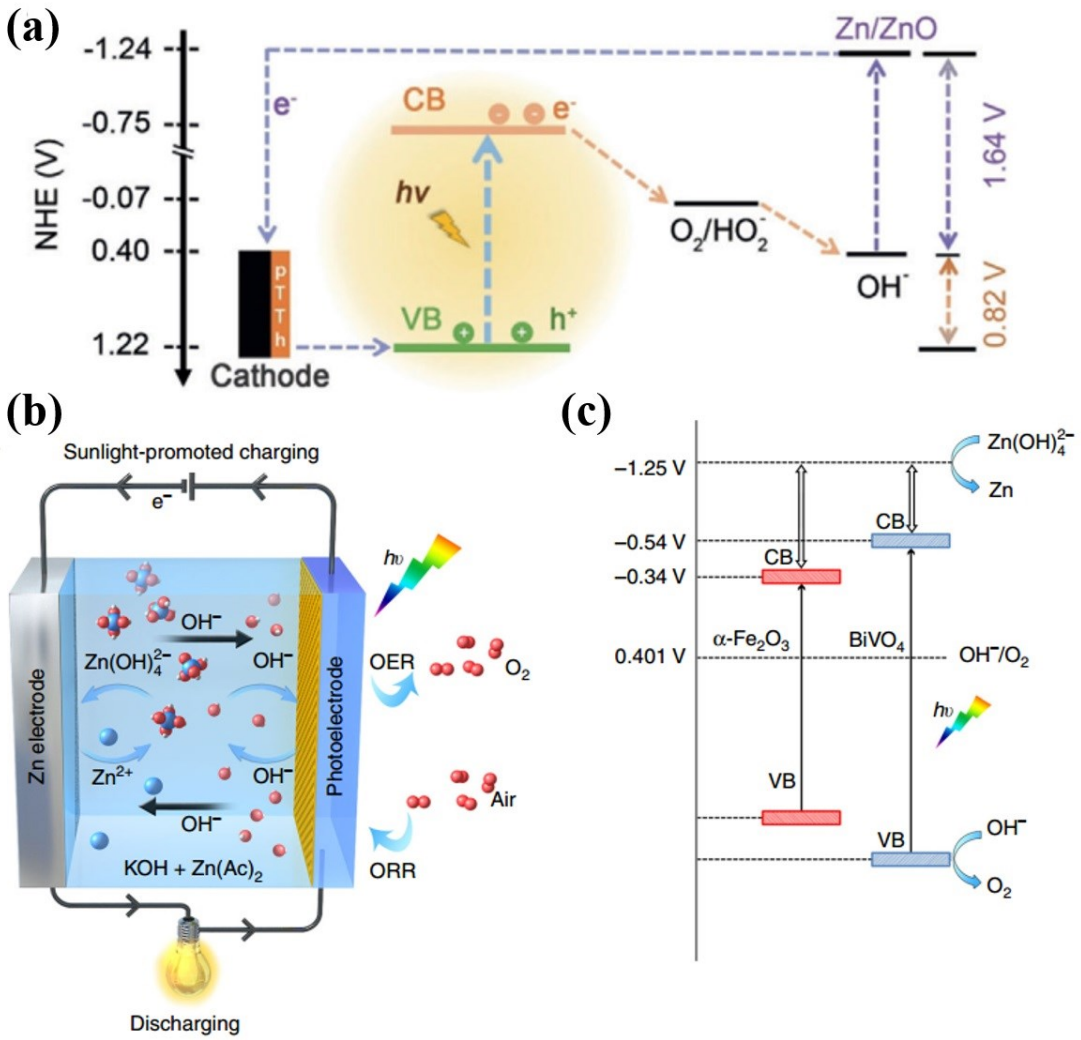

Figure 10. a) Schematic diagram of energy levels for the increased discharge voltage of the Zn-air battery.[111] Copyright 2019, Wiley-VCH. b) Schematic diagram of light-promoted Zn-air battery. c)

Energy band structure of $BiVO_4$ and α-Fe_2O_3 photoelectrodes.[80] Copyright 2019, Nature Publishing Group.

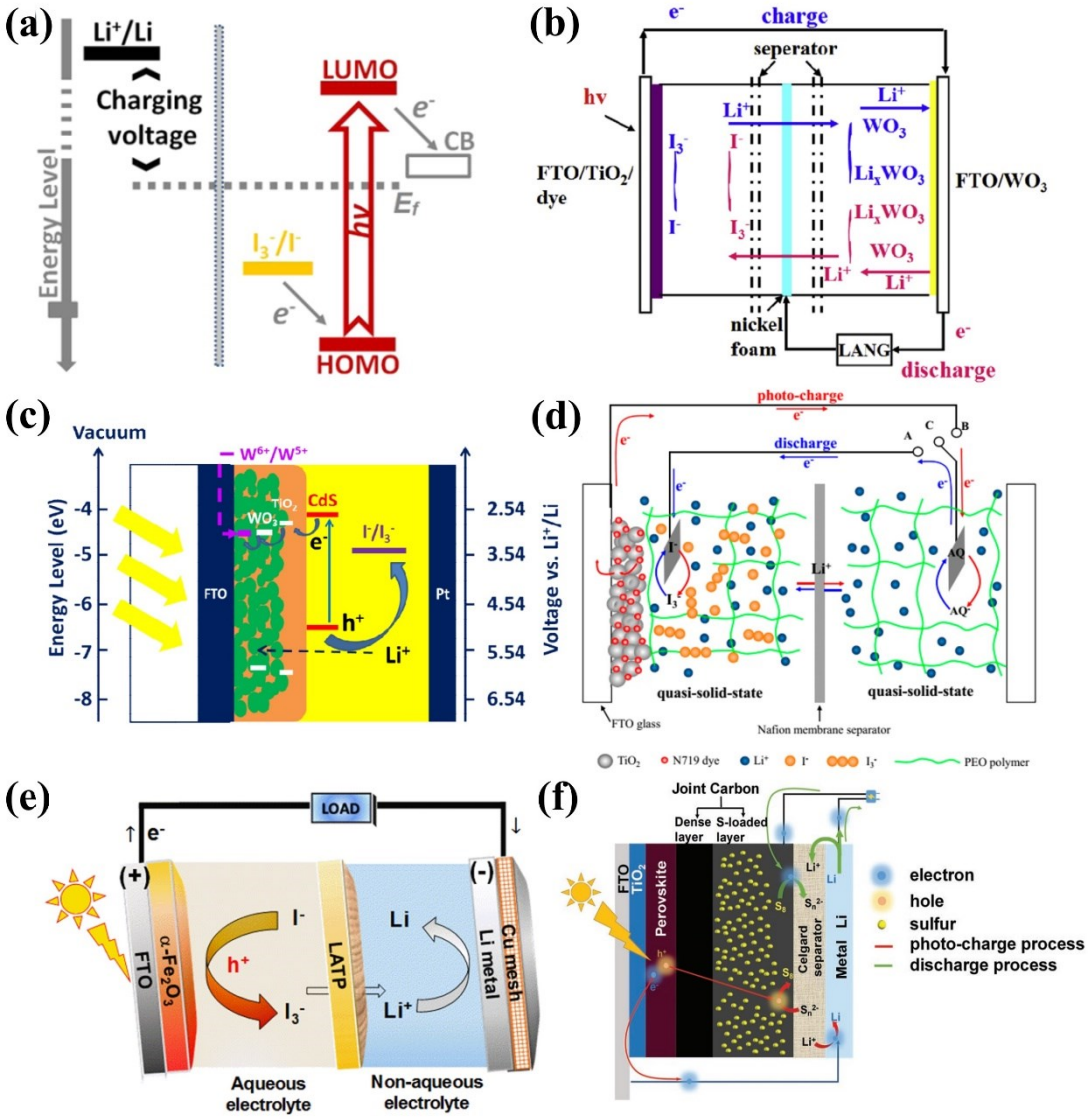

Figure 11. a) Energy diagram for the dye-sensitized TiO_2 photoelectrode based photo-assisted charging process.[114] Copyright 2015, American Chemical Society. b) Scheme of the configuration and working mechanism of the photo-rechargeable battery with WO_3 anode.[115] Copyright 2017,

Elsevier B.V. c) Schematic depiction of the photo-battery based on CdS-sensitized WO_3.[117] Copyright 2018, WILEY-VCH. d) Configuration and electron transfer scheme of the designed quasi-solid-state solar rechargeable battery with PEO gel electrolyte.[118] Copyright 2019, American Chemical Society. e) Photo-assisted charge process in aqueous $Li–I_2$ cells using a hematite photoelectrode (α-Fe_2O_3/FTO substrate).[120] Copyright 2016, American Chemical Society. f) Schematic diagram of the fabricated PSC-Li-S battery.[123] Copyright 2019, WILEY-VCH.

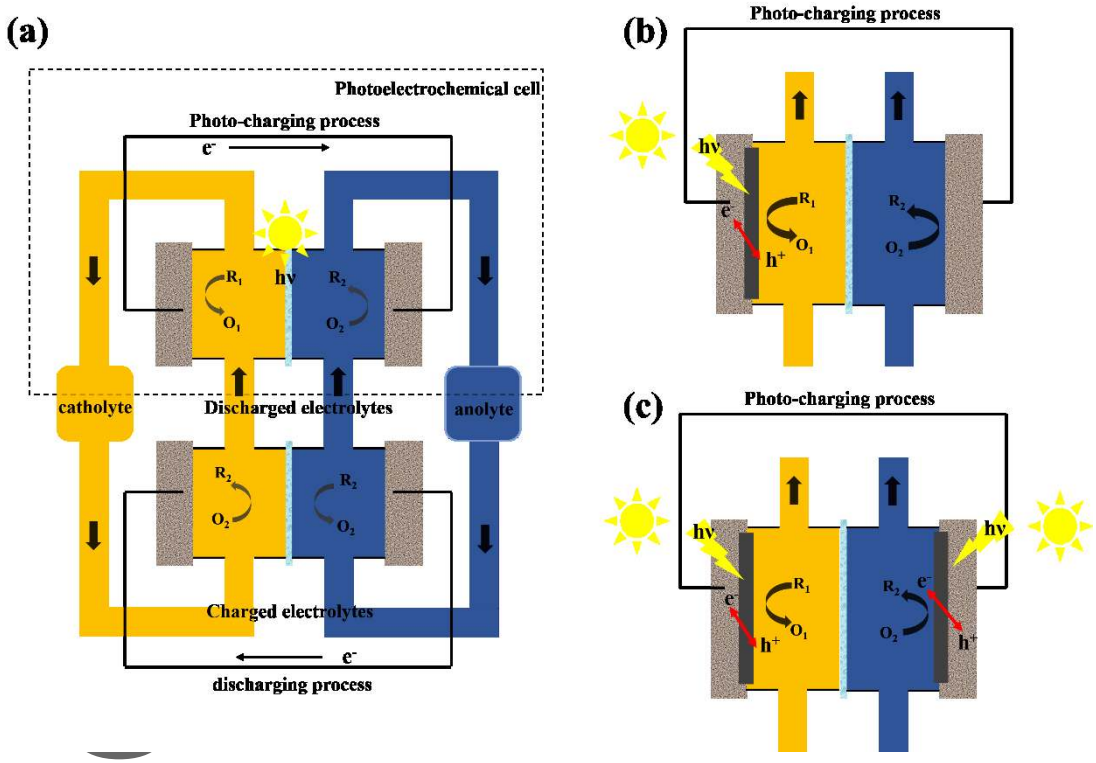

Figure 12. a) Configuration for a Photo-rechargeable RFB and illustration for the photo-charging process with b) single side and c) dual-side photo-charging.

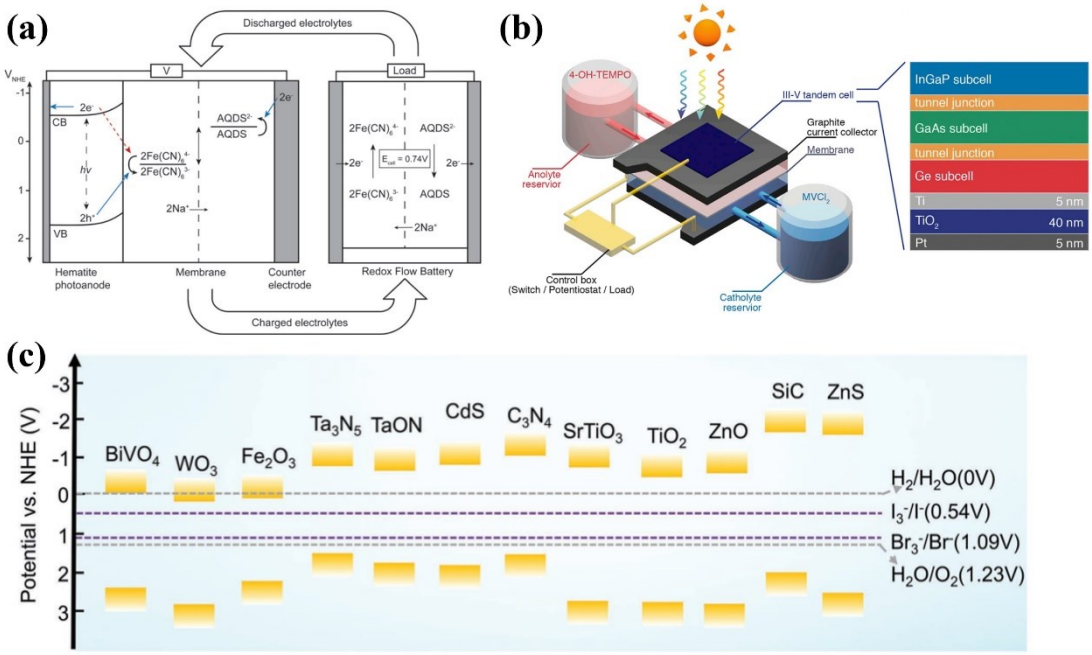

Figure 13. a) Energy diagram of the photoelectrochemical cell for solar charging, and of electrolytes connected to an RFB for discharge. Desired electron-hole pathways under light exposure are shown with full blue arrows. Undesirable back-electron transfer is shown with red dotted arrow.[130] Copyright 2016, Wiley-VCH. b) Integrated photo-RFB device using III-V tandem cell photoelectrode and 4-OH-TEMPO/$MVCl_2$ redox couples.[132] Copyright 2018, Elsevier B.V. c) Relationship between band structures of several photocatalysts and Br_3^-/Br^- and I_3^-/I^- redox potentials of redox couples.[134] Copyright 2018, Wiley-VCH.

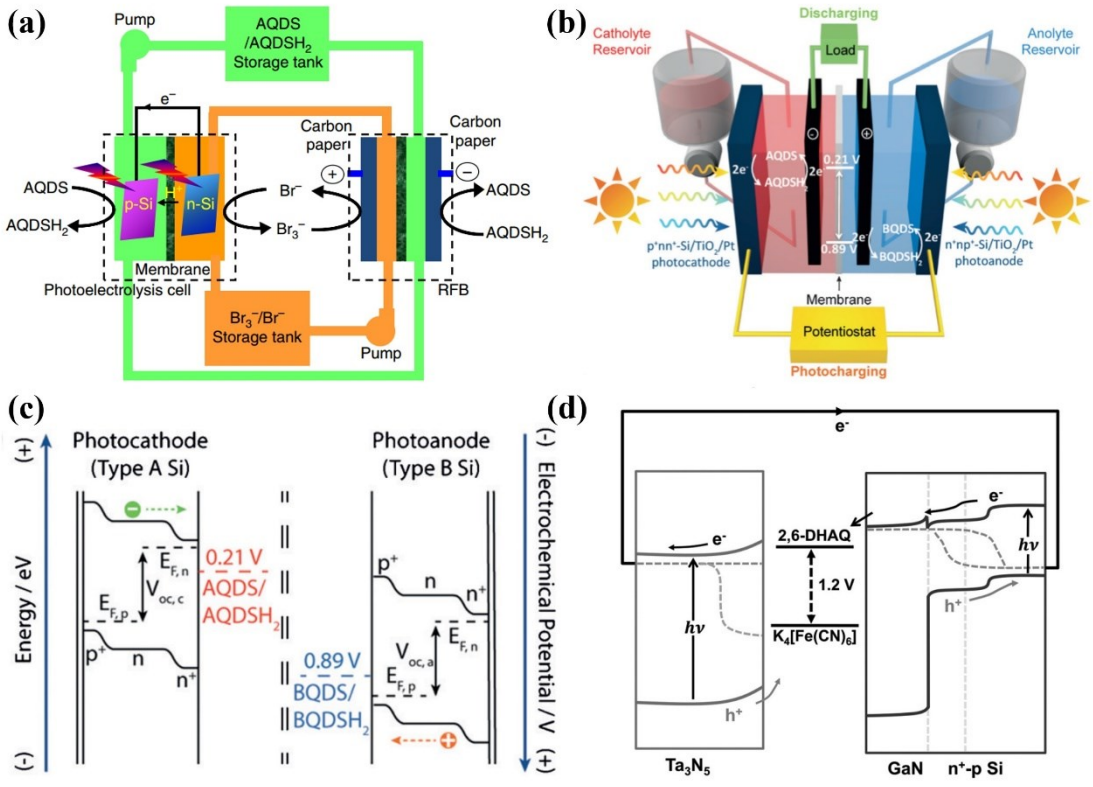

Figure 14. a) Schematic configuration of the proposed SRFC. AQDS/$AQDSH_2$ and Br_3^-/Br^- are used as redox couples.[138] Copyright 2016, Nature Publishing Group. b) Schematic illustration of quinone redox couples and dual Si photoelectrode based photo-RFB. c) Band diagram for the photo-charging process. Type A: p^+ n n^+-Si/Ti/TiO_2/Pt photocathode, type B: n^+ n p^+-Si/Ti/TiO_2/Pt photoanode.[139] Copyright 2016, Wiley-VCH. d) The energy band diagrams of two photoelectrodes (Ta_3N_5 as the photoanode and GaN/Si as the photocathode) and two electrolytes.[142] Copyright 2017, Wiley-VCH.

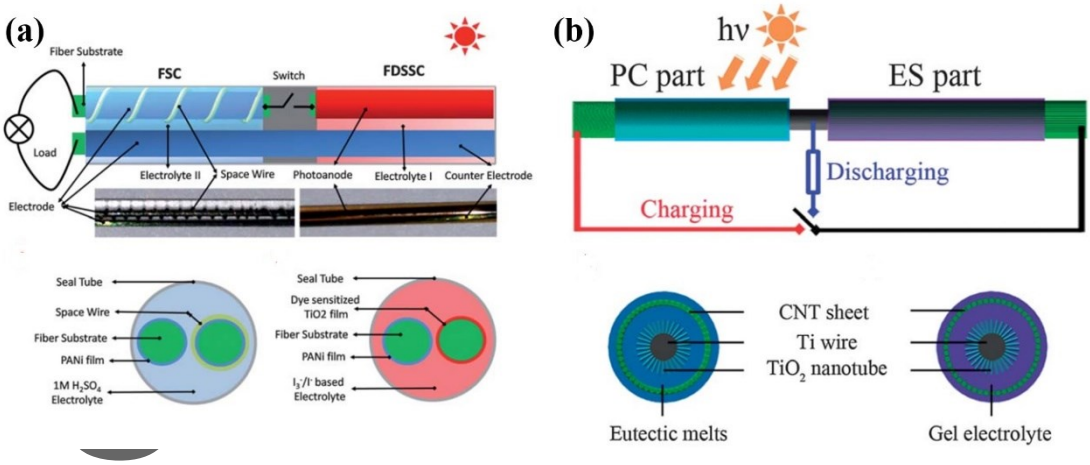

Figure 15. a) Structural schematic and photograph of an integrated energy wire consisting of a fiber-DSSC and a fiber-SC.[11] Copyright 2013, The Royal Society of Chemistry. b) Schematic illustration of the structure of integrated energy wire, and corresponding sectional view is shown below.[144] Copyright 2014, The Royal Society of Chemistry.

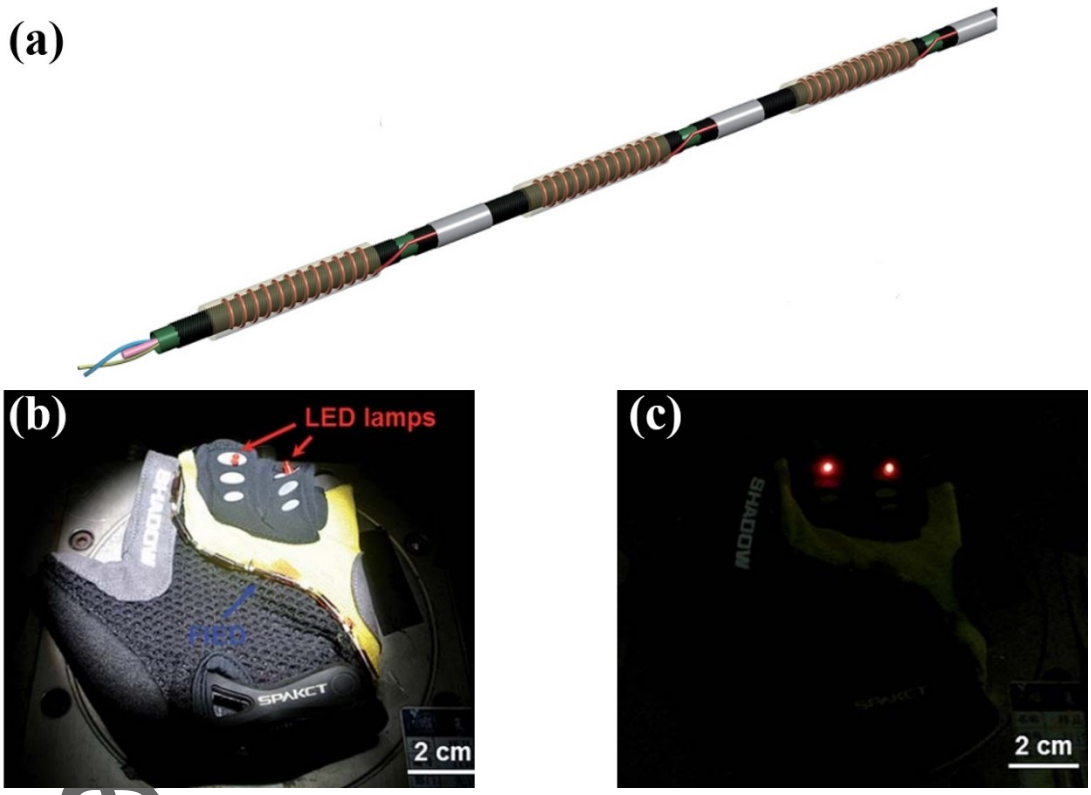

Figure 16. a) Schematic illustration to the fabrication process of the integrated energy wire. b) and c) Photographs of an energy wire being woven into a sport glove for photocharging (under AM1.5 illumination) and powering two light emitting diodes in the dark, respectively.[145] Copyright 2016, The Royal Society of Chemistry.

Table 1. Several of reported photocapacitors based on solar cells.

Solar cell	Charge storage materials	Characteristics	$\eta_{overall}$	Ref
DSSCs	Activated carbon	Two-electrode configuration, where Dye-coated TiO_2 layer attached activated carbon directly	/	[15]
	Activated carbon	Three-electrode configuration, with a Pt electrode contacting with activated carbon directly	/	[18]
	MWCNT, MWCNT–PANI films	The MWCNT film acted as common electrode replacing Pt electrode	5.12% for MWCNT 4.29% for MWCNT–PANI	[20]
	Graphene nanoplatelets	Flexible configuration	1.02% 1.46% at 0.3 Sun	[21]
	Reduced graphene oxide	Flexible configuration with array of three DSSCs could be charges to ~1.8V	/	[22]
	PProDOT-Et_2 conducting polymer	Thick PProDOT-Et2 films possessed higher electrode specific capacitance than PEDOT	0.6%	[25]
	PEDOP@MnO_2 films	PEDOP@MnO2 films simultaneously acted as catalytic electrode for DSSCs delivering a PCE of 6.11%	/	[26]
	PVDF/ZNWA	Pt/Au catalytic electrode was modified by PVDF/ZNWA nanocomposites to realize charge storage	3.7%	[30]
	SDS-modified PVDF	SDS modification enhanced the dielectric constant of PVDF	3.78%	[31]
	PEDOT and ClO_4^- doped	PEDOT acted as catalytic electrode for DSSCs	0.1%	[32]

	PPy	and charge storage electrode simultaneously; Ppy acted as counter electrode of SC		
	Double-sided TiO_2 nanotube arrays	Plasma-assisted hydrogenation treatment enhanced areal capacitance	1.64%	[35]
	Double-sided TiO_2 nanotube arrays	Flexible configuration CuS acted as catalytic electrode for DSSC delivering a PCE of 7.73%	6.5%	[36]
	$RuO_x(OH)_y$	Solid-state DSSC with polymeric hole conductor P3HT	0.8%	[37]
PSCs	PEDOT-carbon composite electrode	The PEDOT-carbon electrode was doped by ClO_4^-, with fast charge–discharge kinetics;	4.7%	[45]
	CNT	CNT bridge effectively prevented the $CH_3NH_3PbI_3$ from degrading	0.77%	[47]
	Nanocarbon materials	High operation voltage of 0.91 V	7.1%	[42]
	Nanoporous carbon	All-inorganic $CsPbBr_3$ PSC; Silica-gel-electrolyte based SCs	5.1%	[48]
OSCs	CNT network	P3HT:PCBM BHJ OSC with a PCE of 3.39% and V_{oc} of 0.6V	/	[50]
	Graphene	Eight series connected P3HT:PCBM BHJ OSCs provided a high V_{oc} of ~5V	/	[53]
	PEDOT:PSS	Foldable integrated photocapacitor Large area P3HT:ICBA BHJ OSC	2%	[54]
	Carbon-black	PCDTBT: $PC_{71}BM$ BHJ OSC reached a PCE of 7.6% under indoor condition	2.92%	[55]

Graphene oxide	Polymer electrolyte (PVA/H_3PO_4) for SCs	5.07%		[56]
	PTB7-Th: $PC_{71}BM$ BHJ OSC reached a PCE of 9%			

Table 2. Several of reported photo-rechargeable static batteries.

Static battery	Battery materials	PC unit	Features of PC	$\eta_{overall}$	Ref.
Li-ion battery	Cathode: $LiCoO_2$ Anode: Li_xTiO_2	Tandem DSSC	V_{oc}= 3.39V	0.82%	[84]
	Cathode: $LiFePO_4$ Anode: $Li_4Ti_5O_{12}$	Triple-junction Si solar cell	J_{sc}=2.0mA cm^{-2} V_{oc}=2.09V	8.5%	[85]
	Cathode: $LiCoO_2$ Anode: $Li_4Ti_5O_{12}$	25 units of c-Si solar cells	Output voltage of 14.1V	7.61%	[86]
	Cathode: $LiFePO_4$ Anode: $Li_4Ti_5O_{12}$	Four PSCs in series	J_{sc}=4.82mA cm^2 V_{oc}=3.84V PCE=12.65%	7.8%	[87]
	Cathode: $LiMn_2O_4$ Anode: $LiTi_2(PO_4)_3$	$Cs_{0.05}FA_{0.81}MA_{0.14}PbI_{2.55}Br_{0.45}$ PSCs	J_{sc}=19.6mA cm^2 V_{oc}=1.1V PCE=16.8%	9.25%	[88]
	Cathode: $LiFePO_4$ Anode: Li metal	TiO_2 photoelectrode connected with $LiFePO_4$ electrode	Reducing charging voltage	/	[79]
	Cathode: $LiFePO_4$	$LiFePO_4$ electrode mixed	Photo-assisted delithiation of	0.08%	[89]

	Anode: Li metal	with dye molecules	$LiFePO_4$		
	Half cell Li_xTiO_2 electrode	Li_xTiO_2 electrode	Li-ion deinsertion reaction under photoexcited	/	[93]
	Cathode: perovskite Anode: Li metal	2D perovskite as photoelectrode	Photo-charged voltage of nearly 3V	0.034%	[95]
Na-ion battery	$Fe_2(MoO_4)_3$ Na ions storage electrode	Dyed-TiO_2 photoanode	Stable photo-charged battery voltage of 0.63V	/	[97]
	NaI_3/NaI and Na_2S_4/Na_2S redox couples	TiO_2 photoelectrode	Reducing charging voltage to 0.07V by photo-assisted	/	[98]
	Anode: SnS_2	SnS_2 photo-cathode	capacity augmentation of 2.5-fold under illumination	/	[99]
Al-ion battery	Cathode: Graphite Anode: Al metal	PSCs module including three connected identical PSCs	V_{oc}=3.28V PCE=18.5%	12.4%	[101]
Li-air battery	Triiodide/iodide redox shuttle	Dye-sensitized TiO_2 photoelectrode	Reducing charging voltage under illumination	/	[105]
	Triiodide/iodide	g-C_3N_4 photoelectrocatalytic electrode	Achieved low charging voltage of 1.9V	/	[107]
Zn-air battery	Cathode: pTTh	pTTh photoelectrode	Photo-inducing ORR at the pTTh cathode; Increasing discharge	/	[111]

			voltage to 1.78V		
	Cathode: $BiVO_4$ or α-Fe_2O_3	$BiVO_4$ or α-Fe_2O_3 photoelectrode	Decreasing charging voltage	/	[80]
Li-I battery	Anode: Li metal I_3^-/I^- based catholyte	Dye-sensitized TiO_2 photoelectrode	Reducing charging voltage by TiO_2 photo-assist	/	[114]
	Anode: WO_3	Dye-sensitized TiO_2 photoelectrode	Charging process was totally accomplished by photoelectrode	/	[115]
	Anode: AQ gel electrolyte	Dye-sensitized TiO_2 photoelectrode		0.3%	[118]
	Anode: Li metal	α -Fe_2O_3 photoelectrode	Delivered a charging voltage of ~ 3.43 V	/	[120]
Li-S battery	Anode: Li metal	PSCs module (three PSC units) in series	V_{oc}=2.8V PCE=12.38%	5.14	[123]

Table 3. Comparison of three types of photo-rechargeable ESS

EESs	PC units	Effect	Superiority	Overall efficiency	Application
SCs	Solar cells	Fully photo-charging	Charged at a fast rate	Over 7%	Stabilizer for solar cells, Wearable Electronics
	Photoelectrodes	Fully photo-charging	Charged at a fast rate Simple configuration	Still low Rarely report	

Batteries	Solar cells	Fully photo-charging	High volumetric energy density. Better energy matching	Over 12%	Self-charged portable power sources
	Photoelectrodes	Photo-charging or photo-assisted charging	High volumetric energy density. Photo-assist reduces overpotential	Still lower 1%	
RFBs	photoelectrodes	Photo-charging or photo-assisted charging	High energy capacity	Reach 14%	Photovoltaic energy storage station

Fangyang Liu received his BS in 2006 and PhD in 2011 from Central South University, where he then worked as a lecturer and associate professor. In 2013, he joined Martin Green's Group at University of New South Wales, Australia as a postdoctoral fellowship. In 2017, he moved back to Central South University as a full professor. His research interests are inorganic solar cells and lithium-ion batteries.

Lianzhou Wang is Professor at the School of Chemical Engineering and Director of Nanomaterials Centre, The University of Queensland (UQ), Australia. He received his Ph.D. degree from Chinese Academy of Sciences in 1999. Before joining UQ in 2004, he worked at two national institutes (NIMS and AIST) of Japan for five years. Wang's research interests focus on design and application of semiconductor nanomaterials in solar energy conversion/storage systems, including photocatalysts and photoelectrochemical devices.

Martin Green is Scientia Professor at the University of New South Wales, Sydney and Director of the Australian Centre for Advanced Photovoltaics, involving several other Australian Universities and research groups. His group's contributions to photovoltaics include inventing the PERC cell, now the main commercial solar cell, and holding the record for silicon cell efficiency for 30 of the last 37 years.

TOC

This review summarizes the development of several types of mainstream integrated photo-rechargeable energy storage systems (ESSs) and introduces different working mechanisms for each photo-rechargeable ESS in detail. Moreover, matching of parameters between photoelectric conversion (PC) and ESS are emphatically discussed. At the end, several perspectives on the future development of photo-rechargeable ESSs are listed.